Stability Characteristics of a Low-Viscosity Axisymmetric Jet

A THESIS
SUBMITTED TO THE FACULTY OF THE GRADUATE SCHOOL
OF THE UNIVERSITY OF MINNESOTA
BY

Akash Chandrashekhar Dhotre

IN PARTIAL FULFILLMENT OF THE REQUIREMENTS
FOR THE DEGREE OF
MASTER OF SCIENCE

Dr Vinod Srinivasan

February, 2021

Acknowledgements

I appreciate the support and encouragement of many who made this arduous journey possible. My sincerest gratitude goes to my advisor, Dr. Vinod Srinivasan, for his patience, guidance, and countless hours of meetings and discussions that helped me complete this work. I am grateful for Dr. Vinod's constructive feedback and continuous encouragement that have helped me grow as an experimentalist and as a researcher. I would also like to thank my masters committee, Dr. Paul Strykowsi and Dr. Michele Guala, for their time and feedback.

I would like to thank my fellow lab mates, Manish, Sankar, Ankit, Merin, Jinwei, Jinjin, and Peter Zhao for their assistance, encouragement, and for putting up with my glycol spills all year round. I am forever grateful to Ian Wright for all his time and help which made this work possible. I want to thank my roommates, Aditya and Milan, for all their help and support. Additionally, I would also like to thank Daniel Mendonza and Brett Rosiejka for mentoring me during and after my time at Johnson Screens.

Finally, my special thanks goes to Roshan Rangarajan for always motivating me and keeping me company. It was fun working around you and I shall always cherish the uncountable hours we spent in the lab learning, doing homeworks, and above all, talking about our mutual love for chess.

Dedication

This work is dedicated to my better half, Shreya, and to my family back home and here in the States for their unconditional love and support.

Abstract

Studies of low-density jets indicate the existence of instabilities that may lead to self-sustained oscillations, which are characterized by a spectacular breakdown of the jet with rapid mixing. However, most studies do not account for viscous effects that can dramatically alter the flow stability. Understanding how viscosity stratification influences jet instability can help design systems with control over the mixing characteristics. Hence, experiments are performed with a low viscosity, density-matched jet issued into an ambient fluid with higher viscosity. These types of systems are often found in engineering applications such as plasma torches, sewage discharges, jet exhausts, etc., and to some extent, in naturally occurring phenomena such as glacial and lava flows. A study of instabilities and the subsequent breakdown of an axisymmetric jet was carried out over Reynolds numbers, Re, ranging from 400 to 3300, for a range of jet-to-ambient viscosity ratio, M, ranging from 1 to 45. Flow visualization results indicate that viscosity stratification leads to helical modes and a transition to axisymmetric modes is observed. Hotwire anemometry results indicate the existence of sharp peaks in the frequency spectrum that vary as a function of Re and M. The flow visualization and hotwire anemometry results are used as markers to identify the possible existence of a global mode.

Contents

List of Figures

Chapter 1

Introduction

Fluid flows undergo changes and the resulting flows in many such cases have been extensively predicted and studied. These changes in fluid flows can be as dramatic as the transition from laminar to turbulence or as ordinary as wave formation in water bodies. As expected, these are of great interest due to their occurrence in nature and their widespread application in engineering systems. To understand and predict why and how flows behave the way they do under different conditions, Helmholtz, Kelvin, Rayleigh, and Reynolds laid the foundations of hydrodynamic stability concepts during the nineteenth century [Drazin, 2002]. This provided the foundation for tools used to evaluate the onset of instability and the transition to turbulence, leading to many well-defined concepts such as the Kelvin-Helmholtz instability– an interfacial instability between two parallel streams– that explains the occurrence of oceanic thermoclines [Woods, 1969] and billow cloud formations [Drazin and Reid, 1981]. Additional works covered a plethora of cases like, for example, the thermal instability observed in a system with cold fluid on top of a less-dense warmer one leading to Benard convection cells, or the centrifugal instability observed in a Couette flow [Taylor, 1923]. This comprehensive collection of work has also served as a foundation for many trying to study dissimilar, unconfined flows.

While many applications in engineering systems deal with confined flows, an equal number of, if not more, are free shear flows in the form of mixing layers and jets and hence the need to study it pointedly. Historically, these studies have often neglected viscosity and as such, the present work explores the effects of viscosity on the stability

of an axisymmetric jet in a free shear flow. A systematic study of the jet to characterize the instabilities seen as convective or absolute has been conducted, and the possible existence of a global mode due to viscosity stratification is theorized.

The effect of viscosity stratification can be dramatic on flow stability; acting to either enhance or curb the growth of instabilities. Also, viscosity is too important a parameter to neglect with viscosity stratification occurring due to any variations in compositions, temperatures, or pressures. Such variations are obviously very commonly found in nature in glacial, pyroclastic, or even atmospheric and oceanic flows. In engineering systems like plasma torches, viscous instabilities can lead to reduced temperatures and consequently, poor coating qualities. Often in sewage discharge systems, the issuing waste into the water body has a different composition/temperature and hence, there exists a viscosity stratification. Here, viscous instabilities that enhance mixing are desirable to avoid high localized effluent concentrations which can be detrimental to aquatic life. In the case of a jet exhaust system, it is clear that the exhaust is a low-density jet being issued into a higher density ambient, a configuration that can be unstable leading to a loss of thrust, but this is not observed. Understanding the precise role of viscosity in the stability of flows can help design systems with control over the mixing characteristics. This work attempts to address the gap in our understanding of the stability of viscous jets by experimentally investigating a low viscosity, axisymmetric jet injected into a more viscous ambient, and by later comparing these results with stability calculations.

Chapter 2

Background

2.1 Basic Concepts– Overview of Stability Theory

This chapter serves to introduce the basic concept of hydrodynamic stability by providing an intuitive example in the form of a mechanical system. Since the present work intends to explore the effects of viscosity stratification on the stability of a jet, previous pertinent studies that explore the stability of systems with or without considering viscous effects have been reviewed.

Intuitively, stability, in a general sense, is easy to comprehend. A system's response to external disturbances determines its stability. By way of example, a sharp pencil, commonly seen lying horizontally on a flat surface, is said to be in equilibrium or a stable state. Theoretically, it is possible to balance a sharp pencil vertically on its point but this configuration is susceptible to a small disturbance, which ultimately will knock the pencil over to its 'stable' state. This vertical arrangement of the pencil can be considered to be unstable. If the other end of the pencil is assumed to be flat, the pencil, with relative ease, can be balanced vertically on its end. An infinitesimal disturbance now may not knock the pencil over but a sufficiently large disturbance will change the stability of the object; knocking it over to a horizontal position. Such a system is termed as nonlinearly unstable.

Using this analogy in fluids, the study of stability of fluids is concerned with the response of a 'base state' to disturbances. If the flow returns to its base state after being subjected to a disturbance, the flow is said to be stable, whereas if the initial flow

breaks down (may lead to turbulence or another steady state), it is said to be unstable. Like in the example discussed above, it is possible for the disturbance to result into a new state. Further, these new stable states can be unstable to other disturbances which then lead to another new stable state and so on. Certain conditions like the critical Reynolds number in a viscous flow or the Richardson number in a stratified shear flow also govern the stability of the system and stability theory deals with the mathematical analysis of the growth or decay of these infinitesimal disturbances.

Instability and the transition to turbulence are studied through laboratory experiments, numerical simulations, linear stability theories, bifurcation and chaos, and nonlinear stability theories [Drazin, 2002]. In the widely used linear stability theory, predicting whether a flow is stable or unstable is found by introducing an infinitesimal perturbation on a base flow and determining if the equations of motion (Navier-Stokes equations) predict the growth or decay of these small disturbances. Note that the disturbances are assumed to be small to ensure linearization is possible to produce analytical results. This greatly limits the applicability of the linear stability theory because nonlinear effects become important when the disturbance velocities grow to some comparable value of the base flow, and real flows also exhibit nonlinear behavior. Despite these apparent disadvantages, the linear stability theory is an important tool used to detect physical growth mechanisms and understand the initial behavior of disturbances. It has had great success in predicting dominant modes since the initial growing disturbance likely out-competes to dominate the flow later. This theory has had excellent agreement between experimental and theoretical predictions on the onset of Tollmien-Schlichting waves and secondary flow in Couette flow [Kundu et al., 2012]. Many real flows such as mixing layers and jets have a non-uniform velocity profile that changes in the streamwise direction and it is assumed that the streamwise variations are slow over a disturbance wavelength. This important assumption retains the validity of linear stability theory on these spatially developing flows by arguing that the velocity profile remains parallel over small distances of the order of a disturbance wavelength [Huerre and Monkewitz, 1990]. As such, the linear stability theory would not be applicable in situations when the disturbances are larger than the spatial variations in the flow.

Mathematically, linear stability analysis consists of superimposing an infinitesimal disturbance on background initial flow, also known as the basic flow [Kundu et al.,

2012]. This disturbance is of the form

$$u(x, y, z, t) = u(z)exp(ikx + imy + \sigma t) \tag{2.1}$$

where $u(z)$ is the complex amplitude of the disturbance wave, $i = \sqrt{-1}$ is the imaginary root, and k, m are the streamwise and spanwise disturbance wave numbers respectively. Here, σ is also known as the temporal growth rate, given by $\sigma = \sigma_r + i\sigma_i$. The complex phase speed of the disturbance is denoted by c, where $c = c_r + ic_i$. The real part of all these quantities produces the physical quantities of interest.

The behavior of the system is then analyzed for all possible wavenumbers, and the stability of the flow is determined by the temporal growth rate. If the value of σ is greater than zero, the system is said to be unstable and if it is less than zero, the system is said to be stable. A special case of marginally stable flow arises when the value of σ_r is zero where the system is on the border and any small change in parameters pushes the system into either the stable or unstable regime. In summary, temporal analysis yields,

$$\sigma_r < 0 \text{ stable state}$$
$$\sigma_r > 0 \text{ unstable state}$$
$$\sigma_r = 0 \text{ marginal state}$$

Stability of a flow can also be defined using the kinetic energy approach [Joseph, 1976] where the evolution of the initial perturbation is studied by measuring its size. The kinetic energy of the disturbance contained in a chosen volume is used to measure its size. A system is said to be stable if

$$lim_{t\to\infty}\frac{E_v(t)}{E(t_0)} \to 0 \tag{2.2}$$

where E_v is the kinetic energy of the disturbance at time t and t_0, defined by

$$E_v = \frac{1}{2}\int_V u_i u_i dV \tag{2.3}$$

This implies that the flow is stable if the disturbances decay over time. In many real flows, there exists a threshold energy, $\delta > 0$, such that the system is stable when the kinetic energy of the perturbation is below this value.

When talking about the instability of a flow field, the terms “local” and “global” are commonly used and they refer to the instability of the local velocity profile and that of

the entire flow field respectively. This facilitates the description of the instability of the system as either local instability or global instability. At the local level of description, instabilities are further classified into two types based on how the disturbances travel: convective instability and absolute instability [Twiss, 1951, Landau and Lifshitz, 1959, Huerre and Monkewitz, 1990]. This concept is illustrated by figure 2.1.

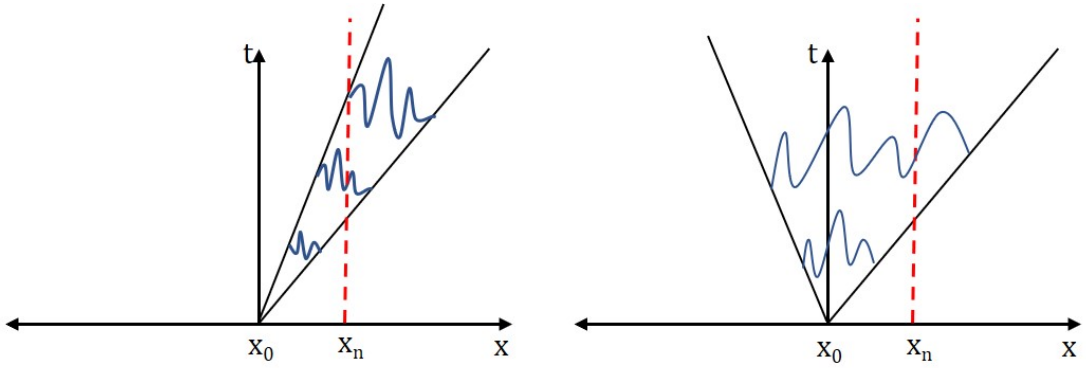

Figure 2.1: Convective instability (*left*) and absolute instability (*right*)

Convective instability is characterized by a disturbance, originating at any point x_0 at time t_0 that grows and travels downstream, as shown in figure 2.1 (*left*). Any particular location x_n downstream will experience this disturbance as it travels through that point but given enough time, will return to its original state. This is in contrast to absolute instability which is characterized by a disturbance, originating at any point x_0 and time t_0, that spreads upstream and downstream, contaminating the entire flow field, as shown in figure 2.1 (*right*). Any location upstream or downstream will experience this disturbance and unlike in convective instability, this disturbance will keep growing to consume the entire domain. Since absolutely unstable flows are self-sustaining in nature, they are said to behave like oscillators. Convectively unstable flows behave like noise amplifiers as the disturbances are amplified and transmitted downstream. Velocity profiles can be convectively unstable or absolutely unstable depending on a number of factors like the shape of the velocity profile, surface tension, viscosity, and density. A necessary condition for the growth of a global mode– a violent breakdown of the flow with a characteristic peak frequency in the spectral content of the flow with relative insensitivity to external forcing– was found to be the occurrence of a finite region of

absolutely instability by some theoretical efforts [Koch, 1985, Chomaz et al., 1991]. The concept of a global mode in terms of a characteristic dominant frequency and the rapid breakdown of the jet is illustrated in figure 2.2.

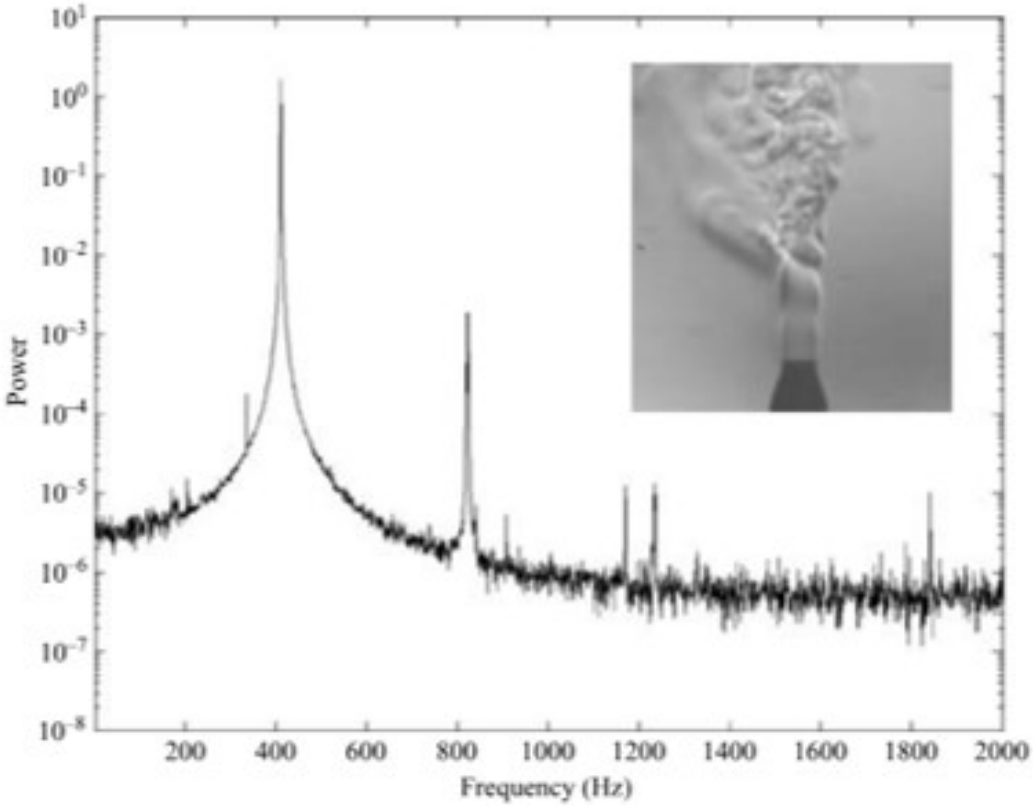

Figure 2.2: Global mode observed in a low-density jet with a jet-to-ambient density ratio of 0.14 at $Re = 650$ and $L/D = 1.5$ [Hallberg and Strykowski, 2006]

2.2 Free Shear Flows

Open or free shear flows, as shown in figure 2.3, usually consists of two interacting streams initially separated by a thin surface. Understanding, and if possible, influencing the downstream evolution of this mixing layer is desirable as such flows are very commonly found in real life applications.

Global modes are well known to exist in closed hydrodynamic systems such as Taylor-Couette flow and many studies have also demonstrated its existence in open systems. Global modes were experimentally observed in wake flows [Provansal et al., 1987, Strykowski, 1986] and a region of absolute instability present in the near wake region of bluff bodies was found to be associated with vortex shedding [Monkewitz and Nguyen, 1987]. Vortex shedding was also shown to be controllable by introducing a smaller cylinder in the near wake region of the main cylinder [Strykowski and Sreenivasan, 1990], through cylinder vibrations [Berger and Wille, 1972], and by heating the main cylinder [Lecordier et al., 1991]. Countercurrent shear layers of an axisymmetric jet [Strykowski and Niccum, 1991, Strykowski and Niccum, 1992] exhibit a global transition when the local velocity profiles in the shear layer are absolutely unstable. Beyond the velocity ratio at which this transition occured, a discrete peak was observed accompanied by suppressed jet mixing.

It was also observed that shear layers in jets exhibit a train of vortex puffs that convect away downstream at high Reynolds numbers [Crow and Champagne, 1971]. These structures surrounding the potential core of the jet interact with each other leading to large-scale structures, and eventually transitioning to turbulence [Wille, 1963]. Winant & Browand [Winant and Browand, 1974] showed that the streamwise development of a mixing layer (coflowing) is predominantly controlled by vortex pairing processes at low and moderate Reynolds numbers. These structures often exchange energy with each other, an example of a nonlinear interaction. A dominant mode therefore arises from these intermediary competing modes.

External forcing is an essential part of studying instabilities in free shear flows as it alters the vortical structures, leading to the excitation of different modes. It is also useful in identifying the existence of global instability that is relatively insensitive to external forcing, as explained later (section 2.3). The development of the flow in space depends on the frequency, amplitude, and phase of all the forcing components. For example, external forcing can produce orderly structures by suppressing background noise and delay the onset of subharmonics produced by vortex pairing [Miksad, 1972]. From an experimental point of view, it maybe useful to have a forced jet as the reference case to eliminate external factors affecting the behavior of the jet. Ho & Huang [Ho and Huang, 1982] demonstrated the effects of a varying excitation frequency on shear

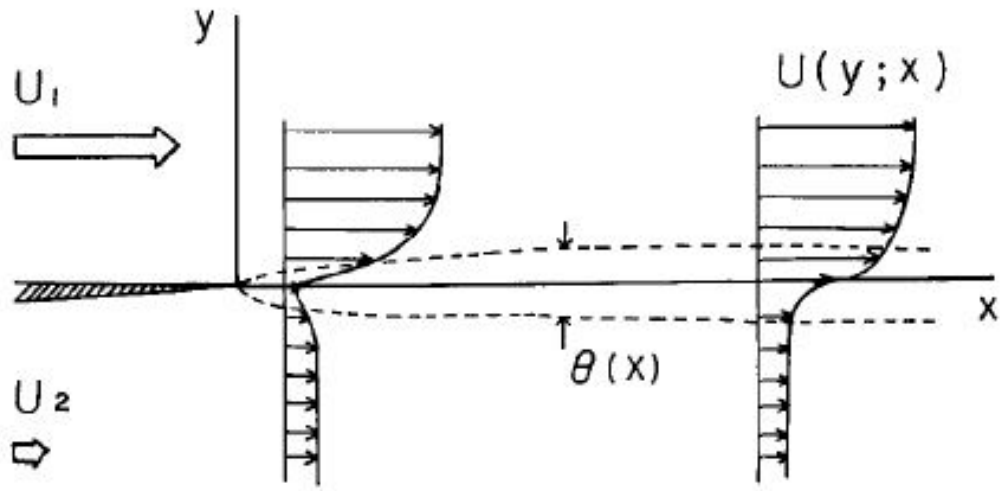

Figure 2.3: Shear layer formed by the merging of two fluids initially separated by a thin surface [Ho and Huerre, 1984]

layers. They observed that the initial vortex formation frequency corresponds to the frequency of the harmonic closest to the natural frequency. Different forcing frequencies lead to either delaying or promoting vortex pairings– which essentially allows for control of shear layer spreading or mixing. Additionally, a small magnitude (0.01-0.1% of the mean flow velocity) of this forcing frequency is sufficient to alter the flow characteristics. This brings along the inherent problem of background noise affecting the flow.

The results of many studies exploring instabilities in free shear flows differ by a large amount due to the sensitivity of these flows to initial conditions inherently present in the facility. Operational parameters such as the velocities of the fluid and ambient, Reynolds numbers, initial state of the boundary layer, background noise, forcing frequency, etc., can greatly affect the stability of these free shear flows [Ho and Huerre, 1984]. A study observed a 100% change in flow characteristics by disturbances levels as low as 10^{-5} in certain regions [Gutmark and Ho, 1983]. Bogey & Bailly [Bogey and Bailly, 2010] numerically demonstrated the sensitivity of round jets to initial conditions. Introduction of random pressure disturbances in the inlet resulted in reduction of the potential core, reduced radial velocity fluctuations in the shear layer, and weaker vortex pairings.

Along with carefully addressing the requirements of a noise-free test facility to produce an initially laminar flow free of any background forcing, experimental studies have

an additional constraint of the inability to decouple initial parameters. Exploring the effects of each parameter requires a large number of experiments and due to poor repeatability, conclusive results are difficult to obtain.

2.3 Instability in Jets

As mentioned previously, some unstable flows display a rapid and catastrophic transition from their steady state, resulting in highly nonlinear oscillations in the flow known as global modes. Identifying whether open flows like jets and mixing layers exhibit global modes and if so, identifying the corresponding region in the parameter space will be helpful in the area of flow control.

Understanding of global modes has partially come through experimental observations of wakes in Karman vortex street as explained in section 2.2, and their existence is also well known in low-density jets. The boundary between convective and absolute instability was initially explored by Monkewitz & Sohn [Monkewitz and Sohn, 1988] and they showed that low-density jets exhibit regions of absolute instability, suggesting the existence of global modes. [Sreenivasan et al., 1989] showed that low-density jets obtained by mixing helium and air exhibit two different types of behavior depending on the density ratios. They also noted an absolute to convective transition by controlling flow parameters. Monkewitz [Monkewitz et al., 1990] used a heated gas to create a low-density jet and their results were in agreement with that of Sreenivasan *et al.* with an additional unstable mode at a higher density ratio. These early studies were primarily focused on analyzing the frequency content of the jets to identify sharp peaks and insensitivity to external excitation– characteristic of global modes. Kyle and Sreenivasan [Kyle and Sreenivasan, 1993] included momentum thickness as one of the control parameters in their study by incorporating the capability of attaching nozzles of different exit diameters. They observed a critical density ratio and momentum thickness value beyond which the absolute to convective transition occurred. Raynal et al [Raynal et al., 1996] also observed self-sustained oscillations in a variable-density plane jet that shut-off after a critical value of density ratio. This work also attempted to explain the disparity between the different values of density ratios, S, at which the transition occurs in low-density jets. Srinivasan et al. [Srinivasan et al., 2010] extended this work

by including subtly different velocity and density profiles, and their results show how stability of a low-density jet is dramatically altered by considering heating and diffusion. A necessary condition for the growth of a global mode was found to be the occurrence of a finite region of absolutely instability by some theoretical efforts [Koch, 1985, Chomaz et al., 1991].

Hallberg & Strykowski [Hallberg and Strykowski, 2006] decoupled the momentum thickness from the Reynolds number by adding extension tubes to their nozzles and their results indicate that the onset of global instability in low-density flows is independent of the density ratio, momentum thickness, and Reynolds number. Jedoubi & Strykowski [Jendoubi and Strykowski, 1994] systematically identified absolute-convective transitions in axisymmetric low-density jets with external co-flow and counterflow and their results were in good agreement with theory, indicating the presence of two modes of absolute instability at different density ratio ranges. Direct numerical simulations of the heated axisymmetric jet configuration used in Monkewitz et al. [Monkewitz et al., 1990], carried out by Lesshaft et al [Lesshafft et al.,], showed the emergence of a nonlinear global mode following absolute instability. However, the frequency of this global mode was different from that of the absolute instability, contradicting the theoretical model of nonlinear global modes. Srinivasan et al. [Srinivasan et al., 2010] extended the previous work on planar jets to axisymmetric jets by including the role of viscosity.

These studies do not fully explain the apparent global mode shut-off behavior observed in low-density jets beyond a point despite satisfying all the typical conditions observed in absolutely unstable flows like low density ratios, high Reynolds numbers, and small momentum thicknesses. Neither has a study explored the independent effects of viscosity on the stability of jets despite the many evidences that viscous effects can contribute to a great extent, even in open flows. This study aims to explore viscous effects in jets to address this gap in literature and builds upon the recent work of Wright [Wright, 2020]. The experimental setup of Wright takes into account all the prerequisites mentioned in the later part of the previous section (2.2) such as an initially laminar jet and the noise-free, “quiet” facility needed to undertake this research.

2.4 Role of Viscosity

As mentioned previously, instability in flows occurs due to the destabilizing effects of surface tension, density gradients, and viscosity stratification. With the basic concepts and the mathematical description of stability laid out, the importance of viscosity and its role in destabilizing the base flow is explained.

Viscous effects have often been neglected in past research but recent studies have demonstrated the vast impact viscosity stratification has on stability. For example, in a channel flow with two fluids of different viscosities, viscous stabilization was observed by the substantial increase in the critical Reynolds number when the viscosity near the wall was decreased [Ranganathan and Govindarajan, 2001] and viscous destabilization in miscible core-annular flows was observed by the onset of instability at extremely low Reynolds numbers ($O \sim 10$) [Selvam et al., 2007]. To understand why the effects of viscosity stratification are so significant, the stability equations are presented here [Sahu and Matar, 2010, Govindarajan and Sahu, 2014].

A unidirectional shear flow $U = U(y)$ is considered along the streamwise direction, x, and wall-normal direction, y. A disturbance of the form

$$u(x, y, z, t) = \hat{u}(z) exp(ikx + imy + \sigma t) \tag{2.4}$$

is superimposed on the base flow. All the flow quantities are expressed in terms of the base flow and the perturbation quantities like velocity, vorticity, and viscosity. For example,

$$(\hat{v}, \hat{\eta}, \hat{\mu}) = (v(y), \eta(y), \mu(y)) exp[i(\alpha x + \beta z - \omega t)]$$

where α, β are the streamwise and spanwise numbers respectively, ω is the frequency and $c = \omega/\alpha$ describes the phase speed of the disturbance. This is then substituted into the linearized Navier-Stokes equation and expressed in normal mode form:

$$\begin{aligned}[v'' - (\alpha^2 + \beta^2)v](U - c) - U''v = \frac{1}{i\alpha Re}\{&\bar{\mu}[v'''' - 2(\alpha^2 + \beta^2)v'' + (\alpha^2 + \beta^2)^2 v] \\ &+ 2\bar{\mu}'[v''' - (\alpha^2 + \beta^2)v'] + \bar{\mu}'[v'' + (\alpha^2 + \beta^2)v] \\ &- i\alpha U'[\mu'' + \mu(\alpha^2 + \beta^2)] - 2i\alpha U''\mu' - i\alpha U'''\mu\}\end{aligned} \tag{2.5}$$

$$\eta(U - c) + \frac{\beta}{\alpha}U'v = \frac{1}{i\alpha Re}\{\bar{\mu}[\eta'' - (\alpha^2 + \beta^2)\eta] + \bar{\mu}\eta' + i\beta U'\mu' + i\beta U''\mu\} \tag{2.6}$$

where $Re = {}^{\rho U_{ref} H}/_{\mu_{ref}}$ is the Reynolds number based on a reference velocity and viscosity. The viscosity of the base state is non-dimensionalized by a reference viscosity like the ambient, for example. The length scale, H, is chosen along the direction of variation (y, here).

Equation (2.5) is also known as the Orr-Sommerfeld equation and equation (2.6) is the Squire equation. The stability of the flow is determined by the value of the imaginary part of the frequency; when $\omega_i > 0$, the flow is unstable. In the Orr-Sommerfeld equation, if the viscosity is assumed to be zero, then it reduces to Rayleigh equation.

The role of viscosity can also be understood using the disturbance kinetic energy, given by

$$\epsilon = \frac{1}{2}\langle u^2 + v^2 + w^2 \rangle \tag{2.7}$$

where angle brackets represent averaging in corresponding directions, and the rate of change of kinetic energy is the net result of production, dissipation, transport, and surface tension. Mathematically,

$$\frac{\partial \epsilon}{\partial t} = \mathcal{P} - \mathcal{D} + \mathcal{T} + \mathcal{S} \tag{2.8}$$

where

$$\mathcal{P} = -\langle \hat{u}\hat{v} \rangle U', \quad \mathcal{T} = \nabla \left[-\frac{\langle \tilde{u}\hat{p} \rangle}{\rho} + 2\frac{\mu}{Re}\nabla\epsilon \right], \quad and \quad \mathcal{S} = \frac{1}{We}\left\langle \left[\hat{v}(\hat{h}_x x + \hat{h}_z z) \right]_{y=\bar{h}} \right\rangle \tag{2.9}$$

Here, $\mathcal{P}$, $\mathcal{T}$, $\mathcal{S}$ denotes the production term stress transport term, surface tension respectively, and $\mathcal{D} = \frac{1}{Re}\langle |\nabla \tilde{u}|^2 \rangle$ is the viscous dissipation term. The viscous dissipation term is always positive which implies that viscosity damps the kinetic energy of disturbances [Hu and Joseph, 1989]. The surface tension term, $\mathcal{S}$, is zero for miscible fluids and the net contribution of the stress transport term, $\mathcal{T}$, is zero [Govindarajan and Sahu, 2014]. Intuitively, viscosity would be considered to have a stabilizing effect and while it is true that viscosity does cause dissipation as mentioned above, it contributes to the production term even more. It is mentioned above that the net contribution of the stress transport term, $\mathcal{T}$, is zero, but it should be noted that it is non-zero locally [Govindarajan and Sahu, 2014]. This means that there is local diffusion of momentum

due to viscosity and this works to change the phase between $\hat{u}$ and $\hat{v}$. When$\hat{u}$ and $\hat{v}$ oscillate out of phase, the production term is zero and hence, the presence of viscosity variation influences the diffusion that in turn affects the phase, production, and ultimately the stability of the flow. Intuitively, it also follows that the effects of viscosity would be small at higher Reynolds numbers due to their inverse relationship, but viscous effects can be large at high Reynolds numbers because they constitute a singular perturbation in the Orr-Sommerfeld equation [Lin, 1946, Drazin and Reid, 1981, Schmid and Henningson, 2001]. At high Reynolds numbers, viscous terms contribute to an O(1) effect and the Rayleigh equation does not produce a correct solutions here– meaning that the effects of viscosity cannot be neglected at these Reynolds numbers. One such region where viscous effects are important is in the vicinity of walls but a study [Craik, 1969] showed that viscous effects in the critical layer, where the perturbation phase speed is close to initial flow velocity ($U \sim c$), alters the stability drastically. Govindrajan [Govindarajan, 2004, Lin, 1946] bolstered this argument by showing that critical layer effects are of the order $Re^{-1/3}$ whereas the wall effects are of the order $Re^{-1/2}$. This demonstrates that the viscous effects cannot not be neglected in confined or open flows. Although the Rayleigh-Fjortoft criteria ([Rayleigh, 1879, Fjørtoft, 1950]) defines the necessary (but not sufficient) conditions for inviscid instability, they also serve as a qualitative indicator for viscous flows. Hence, viscosity variation can alter the base flow and consequently the stability of by introducing an inflection point in the velocity profile.

The importance of viscosity is demonstrated in a constant shear, unidirectional, sharp-interface flow that was known to be neutrally stable to disturbances of any wave numbers according to the invsicid theory. This flow was shown to be unstable for long waves at any Reynolds number [Yih, 1967], from the Orr-Sommerfeld equation. A possible explanation is that the disturbance vorticity creates vortex pairs on either side of the interface that, depending on the configuration, transport fluid from one region to another, thereby stabilizing or destabilizing the flow [Charru and Hinch, 2000]. A two-layer arrangement with a viscosity jump in a plane Poiseuille flow was numerically shown to be unstable to shear mode instabilities [Yiantsios and Higgins, 1988]. A three-fluid core annular flow was shown to be absolutely unstable for Reynolds numbers greater than O(10) and a range of wave numbers [Valluri et al., 2010, Sahu and Matar,

2011]. Experimentally, interfacial instability at high Reynolds numbers was observed in an oil-water channel flow configuration [Charles and Lilleleht, 1965, Kao and Park, 1972]. Experimental observations in a two-layer Couette flow arrangement were also in good agreement with theoretical predictions [Sangalli et al., 1995, Barthelet et al., 1995], reinforcing the fact that viscosity had a role in the destabilizing process. Analytical calculations by Hu & Joseph [Hu and Joseph, 1989] suggested that viscosity destabilized core-annular flows in pipes. This was experimentally confirmed by Aul & Olbricht [Aul and Olbricht, 1990] and numerically by Kouris & Tsamopoulos [Kouris and Tsamopoulos, 2002].

On the other hand, unlike immiscible fluids, not all miscible interfaces are unstable. Planar miscible flows are found to be unstable at high values of viscosity ratio, Reynolds number, or Schmidt number. Similarly, core annular pipe-flows are more unstable as compared to immiscible cases in some ranges of controlling parameters, and more stable in others [Selvam et al., 2007]. Consistent with theory, experimental results of core-annular pipe flow indicate a presence of axisymmetric instability in the form of interesting pearl and mushroom patterns [d'Olce et al., 2008], and corkscrew mode [Cao et al., 2003] at a slightly higher value of m. In the presence of high viscosity ratios, self-sustained oscillations indicating absolute instability were also seen in pipe-flows experimentally [d'Olce et al., 2009] and numerically [Selvam et al., 2009]. These results are a testament to the influence of viscosity on the stability of a flow.

Stability of flows due to density variation has been studied thoroughly and is usually simpler to predict than the effects of viscosity. The effects of viscosity variation has received significantly less attention and while recent studies have addressed the issue, these studies typically look at confined flow configurations. Most real life systems like plasma torches, jet exhaust, sewer systems, etc., deal with open flows and a need for understanding the stability of such flows is critical. This experimental work, coupled with the numerical work currently in progress in the same lab, aims to broaden our understanding of free shear flows.

With a background of the past works established, the experimental facility and technique is explained in detail in the next chapter.

Chapter 3

Experiment

3.1 Objectives

To achieve the overall aim of understanding the effects of viscosity on the breakdown of the jet, intermediate goals are defined and a parameter space is mapped out to cover the regions of interest. These experiments are in continuation of and extend the study carried out in the same lab by Ian Wright and Dr. Srinivasan and hence, are conducted in the same test facility. Additionally, this work also hopes to serve the purpose of validating numerical stability predictions also currently being worked out in the same lab. The objectives are stated before an in-depth discussion about the experimental setup to provide an explanation for the decisions taken, like the choice of fluids, for example.

It is imperative that the viscosity ratio be the independent variable and to ensure that the breakdown is due to viscosity alone, the fluids are chosen such that their densities are the same but produce a high viscosity ratio. In addition to the density ratio which has been eliminated, the literature also suggests that the breakdown of a jet depends on the Reynolds number and the momentum thickness. The Reynolds number is defined by the jet centerline parameters and is given by

$$Re = \frac{\rho * U * d_n}{\mu_{jet}}$$

where ρ is the density of issuing fluid, which is the same as the density of the ambient fluid, U is the jet centerline velocity, d_n is the diameter of the nozzle, and μ_{jet} is the

viscosity of the issuing jet. The momentum thickness, which depends on the nozzle geometry and the Reynolds number is restricted to a function of the Reynolds number only by fixing a nozzle geometry. As mentioned earlier, the onset of a global mode is characterized by a sharp, dominant peak in the frequency spectrum of the jet, a visible change in the appearance of the flow field, and to some extent, an insensitivity to external excitations. Hence, a measurement plan which allows for the capture of the said frequency peaks along with some flow visualization aid to capture the transition is required. Finally, the effects of external forcing on the dominant breakup frequency and the critical frequency of suppression, if any, need to be studied in order to ascertain the existence of global modes. In summary, the objectives of this work can be broken down into the following:

- Isolate the effects of viscosity ratio
- Measure spectral data for varying viscosity ratios in a range of Reynolds numbers from 400 to 3200.
- Map the behavior of the dominant frequency as a function of the viscosity ratio, Reynolds number, and external forcing.
- Visualize mode transitions

3.2 Test Facility

A detailed description of the test facility previously created by Wright [Wright, 2020] is given below. The aim of the test facility is to address the aforementioned requirements. Figure 3.1 shows the schematic of the test facility. Following the description of the test facility, a detailed account of the experimental technique used is provided.

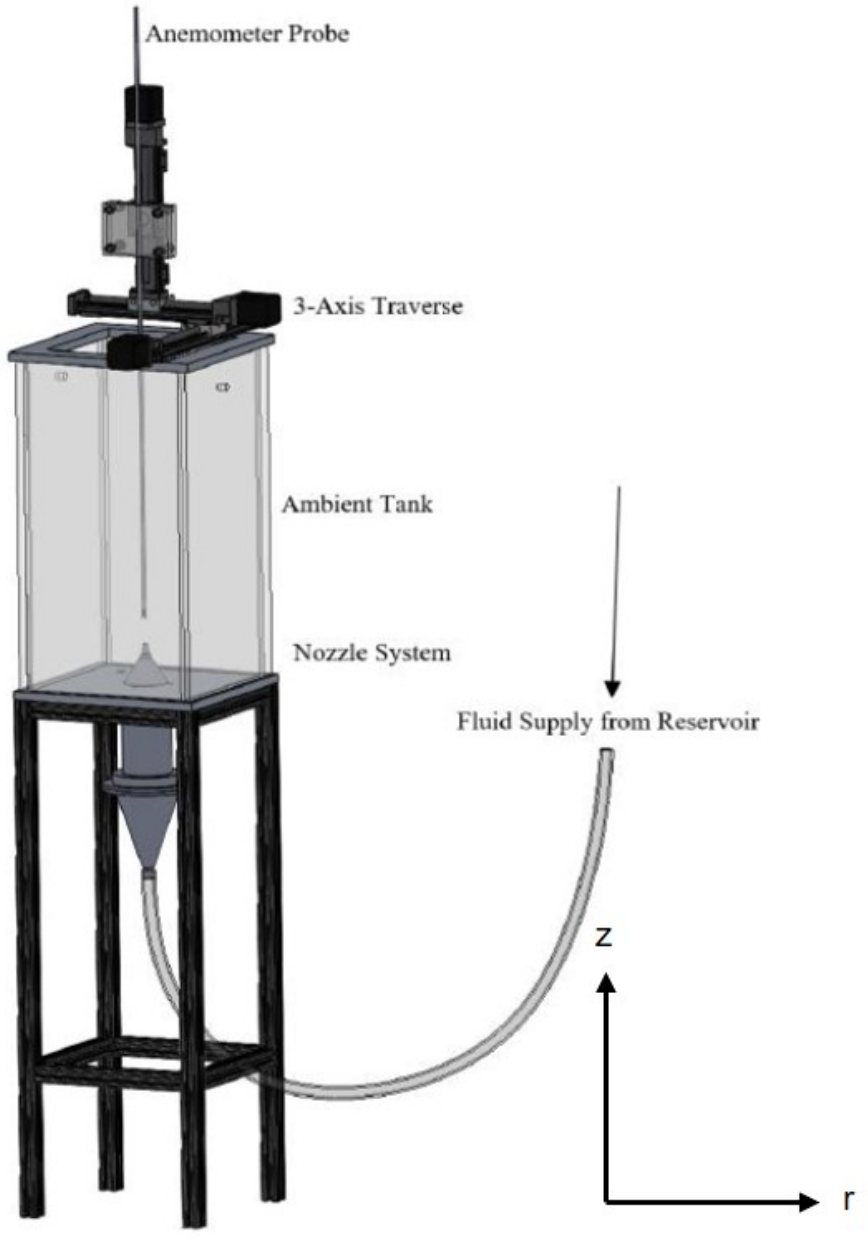

Figure 3.1: Schematic of the test facility [Wright, 2020]

As seen, the setup consists of a large 50-gallon overhead reservoir that contains the fluid to be issued from the jet. A clear acrylic tank– also called the test section– houses the ambient fluid into which the jet is issued through a nozzle at the center of the test section. The walls of this test section are 20 jet diameters ($20 * D$) from the nozzle and the height of the free surface is 65 jet diameters ($65 * D$) from the jet exit plane. This ensures that the flow is unconfined and a semi-infinite domain approximation is satisfied. To avoid altering the flow due to induced vibrations, a gravity-driven flow is preferred over a pump and hence, the reservoir is placed 2 meters above the top of the tank to provide the required head. The large reservoir ensures that the flowrate through the jet is constant throughout a run, even at higher Reynolds numbers. The reservoir is connected to the test section through 1/2 inch Tygon tubing and a Brooks flowmeter is used to control the flow rate of the jet. The reservoir has two drain ports located near the top of the test section that accommodates the incoming fluid and keeps the height of the fluid in the test section constant. Since the breakdown of the jet is dependent on the trailing edge of the nozzle [Ho and Huerre, 1984], it is of utmost importance to have thin nozzle walls and hence, a fifth-order polynomial nozzle with an area contraction of 87:1 and 0.5 mm wall thickness is manufactured using 3D printing. A flow straightener to break up large scale structures along with a diffuser to expand the flow and break up the developed tube velocity profile are incorporated with the nozzle.

3.3 Fluids

The key parameter while selecting the ambient and the jet fluid is the relative density and viscosity of the two fluids. Past studies have often used a helium jet in an air ambient but this selection is ideal for when density ratios are being considered. Additionally, to create viscosity ratios of any significant values, the gases need to be heated to unreasonably high temperatures. Hence, polypropylene glycol, which has a viscosity of $\mu = 0.047$ Pa-s and density, $\rho = 1036.5\ {}^{kg}/_{m^3}$, and saltwater are chosen. The saltwater is prepared by using common salt or Sodium Chloride with water such that the density of the solution is $\rho = 1036.5\ {}^{kg}/_{m^3}$. This particular combination of fluids allows for density matching that effectively negates an important parameter which the stability of the flow depends upon and the stark contrast in the viscosities also allows for a large

range of viscosity ratios (≈ 45), M, which is defined as the ratio of the viscosity of the ambient fluid to the viscosity of the jet. It is expressed as

$$M = \frac{\mu_2}{\mu_1}$$

3.4 Measurement System

3.4.1 Velocity Measurement

Hotwire anemometry is used to measure the velocity of the jet. The anemometry system consists of a probe attached to an IFA 100 anemometer. The probe, manufactured by TSI, is a model $1260A - 10W$ hotfilm probe coated with a thin film of quartz for use in liquids. The hotfilm probe is essentially a small, thin piece of wire connected in a Wheatstone bridge with resistances of known values. The wire is heated electrically and the heat loss due to the fluid stream gives the velocity in terms of a voltage. The hotfilm probe is mounted on a stem that is clamped onto a 3-axis traverse system and these linear stages are controlled by individual Velmex stepper motors. This arrangement allows for the probe to be placed precisely at certain locations using commands to the stepper motors. Although an inherently intrusive technique, the flowfield upstream of the hotfilm probe is unaffected by the presence of the hotwire in the flow, and the measurements thus obtained are considered reliable. To ensure that the measurements near the nozzle walls are accurate, the probe is oriented such that the hotwire is perpendicular to the $r - z$ plane, where r is the radial direction and z is the downstream direction. The entire length of the cable connecting the probe to the anemometer is shielded using Aluminum foil to eliminate electrical interference. Since the hotfilm probe is electrically heated in saltwater, there exists an ionic migration which leads to the deposition of solids on the hotwire. Along with unacceptable data, this also increases the risk of damaging the wire. Hence, care is taken to clean the hotwire with a camel hairbrush and DI water occasionally and the hotwire is always operated under the recommended temperature.

3.4.2 Flow Visualization

Since the most descriptive characteristic of the global mode is a rapid, spectacular breakdown of the jet, a flow visualization to capture the flow physics is essential. The clear acrylic used in the test section construction and the transparent combination of fluids chosen allowed for easy visual access to the jet. A Canon $550D$ camera is placed perpendicular to the light source and such that the near field of the jet was in focus. The jet was initially dyed using food color and a bright LED light source was used to illuminate the dyed jet but this resulted in poor contrast. A fluorescent dye, Rhodamine B, was then used with two bright blue LED light sources on either side of the jet. Since Rhodamine B fluoresces and emits in orange ($\sim 590nm$), a B+W 55 mm Orange MRC 040M Filter is used on the camera. This filter has a 0% transmission rate for wavelengths below $\sim$ 525 nm and hence would produce a completely dark background with excellent contrast for background illumination below the threshold. Both the ambient fluid and the jet were dyed with Rhodamine B and optimal images were obtained with the latter configuration. The images were later post-processed using ImageJ to enhance contrast and produce greyscale images. Particle image velocimetry is currently being integrated into the setup as an alternative flow visualization technique. The advantage of PIV over the current technique is multifold in that it captures the jet breakup as well as the entire flow field. Figure 3.2 shows the flow visualization setup.

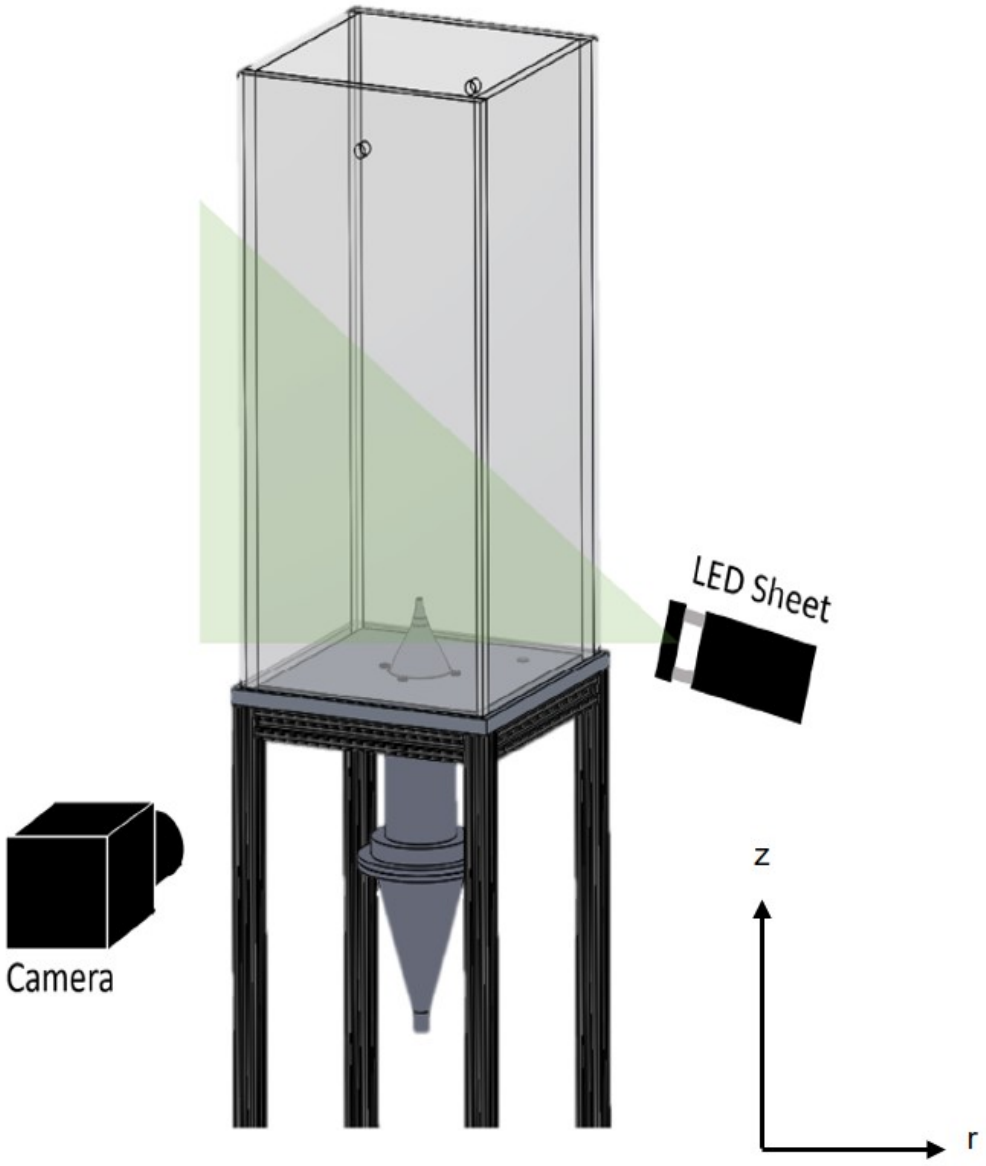

Figure 3.2: Schematic of the flow visualization setup [Wright, 2020]

3.4.3 Data Acquisition

As explained above, the hotwire probe records the velocity data in terms of voltages. These voltage measurements are recorded on a computer through an Agilent 34411A multimeter using a Python program. Additionally, the stepper motor controller also communicates with the same Python program via a USB and NI Visa library.

3.5 Experimental Technique

The experiments are broadly divided into two kinds; flow visualization and hotwire experiments. Since flow visualization experiments required disassembly of the hotwire probe, stem, and clamping arrangement, the two experiment sets are performed independently. Each experimental run consisted of the jet being issued into the ambient fluid at a specific Reynolds number and the hotwire measurements were taken at decreasing values of viscosity ratios. Every trial started with filling the overhead reservoir with salt water, which is made in multiple 5-gallon batches and pumped up to fill the large tank. While the exact amount of sodium chloride in each batch differs due to slightly different quantities of water, the resulting density of the saltwater in the reservoir is the same as that of propylene glycol, rho=1.036, measured using a hydrometer. Due to the nature of the solution, it is easy to adjust the density by adding additional salt/water, which ensures accurate density matching. Some saltwater is drained through the system via the jet to fill up the tubing with saltwater and rid the tubes of air bubbles. Industrial grade polypropylene glycol, with a measured density of rho=1.0365, is used as the quiescent ambient fluid. Care is taken to fill up the test section slowly using a funnel to avoid bubbles. Once the fluids are density matched, the following procedure is followed.

3.5.1 Hotwire Experiments

As mentioned previously, hotwire anemometry aids in velocity measurement at specified locations, and in determining the dominant frequency of the jet. Prior to measuring voltages, the hotwire is calibrated in water using the generalized King's Law, expressed by

$$E^2 = A + B * U^{1/n}$$

where E is the measured voltage, U is the known velocity determined from the flowmeter, and A, B, n are coefficients obtained from the best linear curve fit ($R^2 \sim 0.995$). This equation is then used to determine unknown values of velocities based on voltage measurements. An immediate discrepancy can be noted in U, which is said to be calculated from the flowrate. Such an assumption of U is inaccurate because the velocity profile is not a true top-hat profile and thus, introduces errors in the calibration curve. This was accounted for by correcting the calibration curve using a volume-matching technique explained later on. After calibration, an accurate half jet velocity profile, to calculate momentum thickness, was obtained by measuring velocities every 0.1 mm along the radial direction. The measurement schematic is shown in figure 3.3

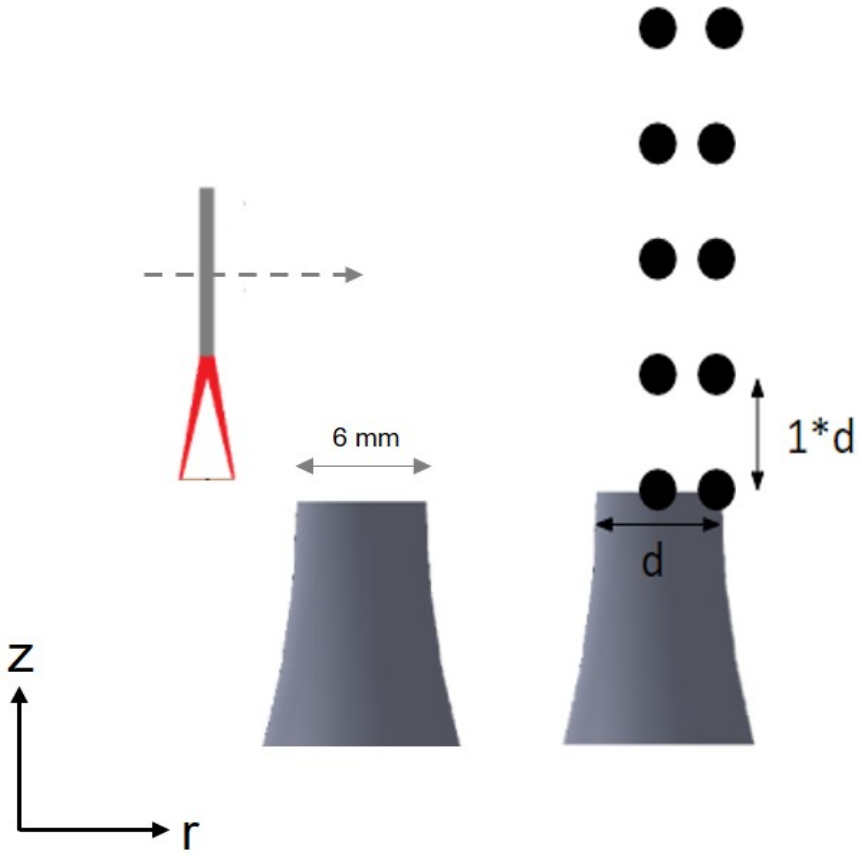

Figure 3.3: Schematic of the hotwire measurement plan

For trials with propylene glycol and salt water, the trial is started at a high viscosity ratio of $M \sim 45$. The saltwater is turned on to achieve the required Reynolds number using the flowmeter and the saltwater jet is allowed to run for a few seconds to reach a steady state before the data acquisition begins. The hotwire starts collecting voltages 2048 times every second, for two seconds at 10 locations. This sampling frequency of 2048 Hz is much larger than the frequencies observed in the jet (17-60 Hz) and reduces aliasing. The probe is programmed such that it measures the velocity fluctuations at five locations, each spaced $1 * D$ apart, along the centerline, then moves over to the shear layer where it repeats the same measurements. Each measurement takes 2 seconds and the probe is further allowed to rest for 1.5 seconds between its travel from one measurement station to another to ensure it is at rest. The viscous ambient also helps in damping the motion of the probe and stem. In total, the measurements take ~ 50 seconds after which the jet is turned off. The saltwater and propylene glycol are mixed with a power drill and a paint mixer carefully to avoid any bubbles, after which the density of the tank is measured using a hydrometer. A small sample of the liquid is collected for later viscosity measurements in the concentric cylinder geometry of a Discovery HR-3 rheometer. The viscosity of the ambient fluid in the tank is lowered due to the addition of the saltwater from the jet and this process is repeated until the desired viscosity ratio trials are finished.

3.5.2 Flow Visualization Experiments

The reservoir is dyed with a small amount ($\sim 1g$) of Rhodamine B and clear propylene glycol is filled into the test section. The light source is placed on both sides of the jet and a B+W 55mm 040M MRC filter is mounted on Canon 550D. The ISO is turned down to 400/800 with the shutter speed set to 1/2000. The camera is mounted on a tripod and operated by a wired remote control to avoid any jitters. The jet is turned on at the desired Reynolds number and pictures are shot on continuous mode until the visibility is ruined by the mixing. The photos are then post-processed in ImageJ to enhance contrast and create image sequences to identify breakup modes. As in the hotwire trials, the tank is mixed carefully after each run to ensure homogeneity, and the trial is repeated for a new value of M. Since the flow visualization trials end quickly on account of decreasing visibility due to mixing, the drop in the viscosity ratio is substantially slow, to the point

where successive trials are almost identical. Another problem is the apparent build-up of dye in the test facility tank which reduces the contrast drastically. These problems were solved by adding predetermined amounts of saltwater in addition to the volume issued by the jet to imitate the decreasing viscosity ratios in hotwire experiments.

Chapter 4

Results and Discussions

4.1 Jet Characterization

The experimental facility designed by Wright [Wright, 2020] produces an axisymmetric jet and the jet breakup is investigated using hotwire anemometry and flow visualization.

Using a hotfilm probe placed at $0.1mm$ above the nozzle exit plane ($0.016 * D$), a velocity profile of the jet was found by traversing the probe in a radial direction outwards, in small increments of 0.1 mm ($0.016 * D$).

Multiple measurements (corresponding to the input sampling frequency, $f = 2048$) are taken at each radial station over a specified time interval ($t = 2seconds$) and the average at each point is considered to obtain the velocity profile of the base flow. Since the velocity profile is measured so close to the nozzle exit, it is essentially disturbance-free and can be assumed to be a true representation of the actual flow. Previously, this facility was restricted to Reynolds numbers of ~ 1500 and was subsequently modified to accommodate for Reynolds numbers up to ~ 5000 while maintaining a flat tophat velocity profile. Figure 4.1 is an example of the measured velocity profile at a $M = 1$ and $Re = 1680$.

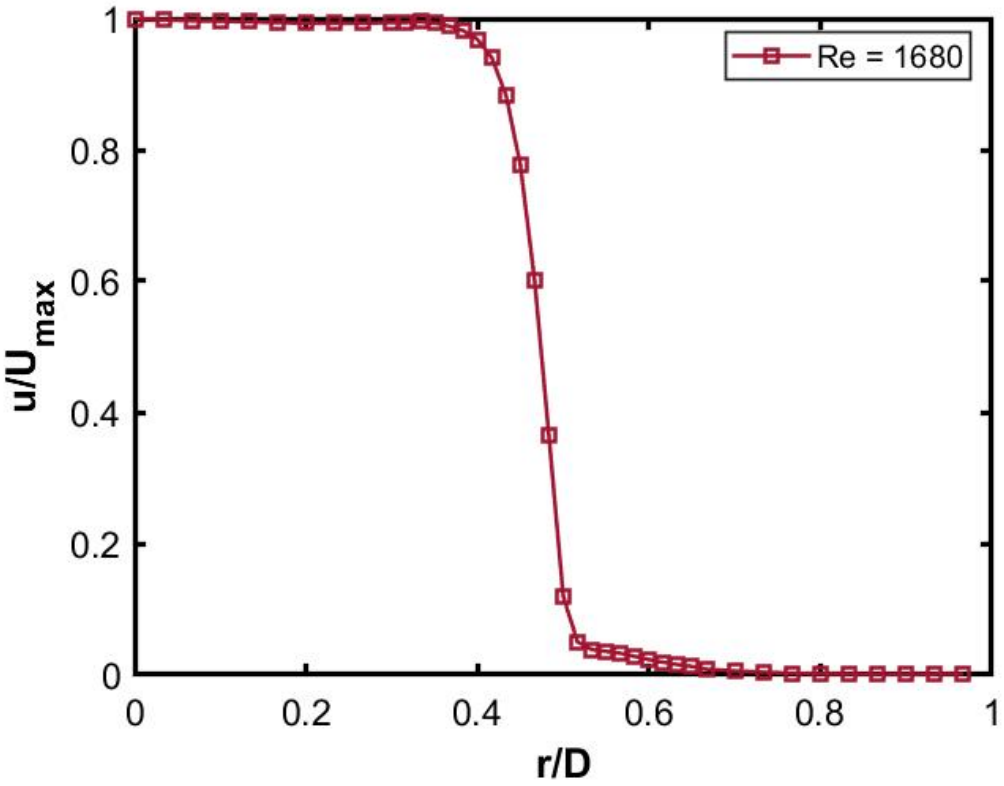

Figure 4.1: Velocity profile measured radially outwards at the jet exit plane for the case $M = 1$ and $Re = 1680$.

A measure of the fluctuations in velocity along the jet velocity profile is shown in figure 4.2. These velocity fluctuations are normalized by the average velocity and describe the turbulent intensity of the jet initially.

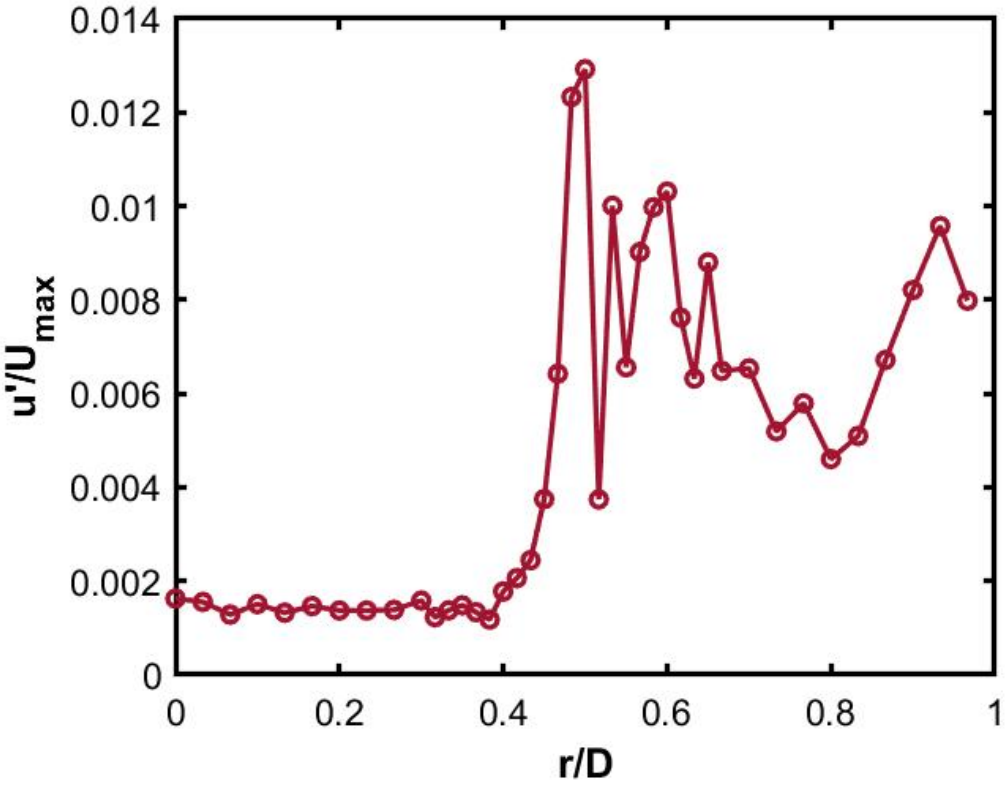

Figure 4.2: Velocity fluctuations measured radially outwards at the jet exit plane for the case $M = 1$ and $Re = 1680$.

The fluctuations in the core region of the jet are very small ($O(0.1)\%$ of U_{max}) as compared to the shear layer, where the turbulent intensity is noted to be about 1.3% of the centerline velocity. This increase in the turbulent intensity near and beyond the nozzle walls is due to the mixing of the jet fluid with the ambient. The self-similar nature of the jet at different Reynolds numbers is noted in figure 4.3. These flow profiles are consistent with the results of Wright (2020) at similar Reynolds numbers and Todde et al [Todde et al., 2009] for low Reynolds numbers free jets.

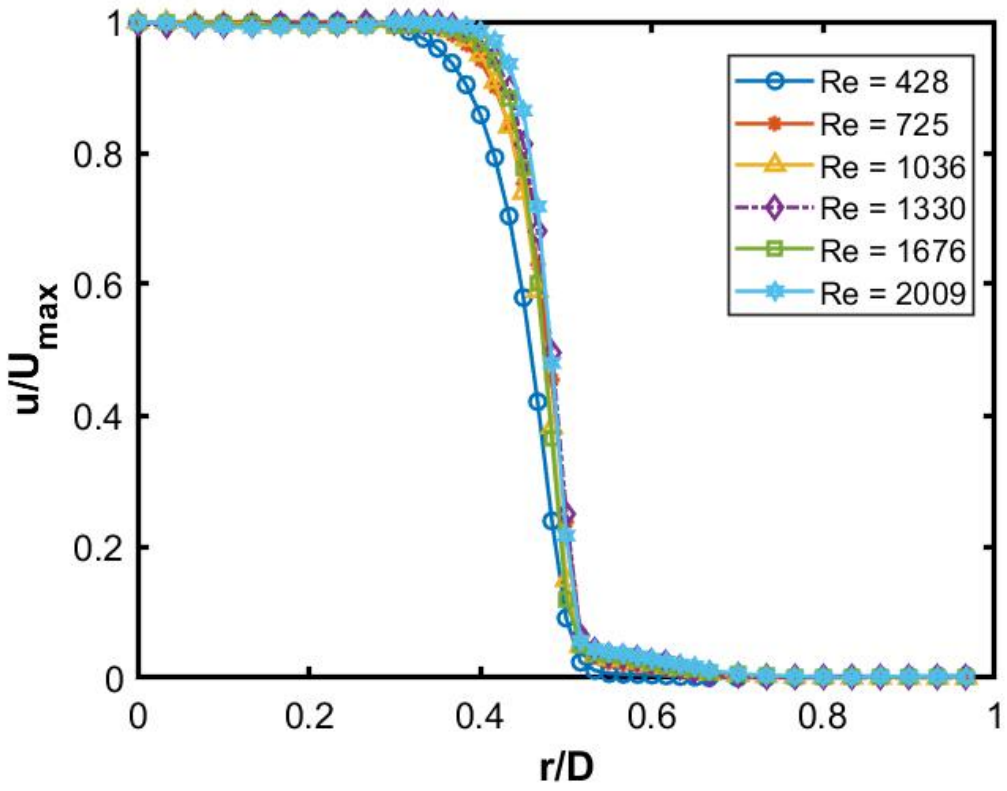

Figure 4.3: Measured normalized velocity profiles at the jet exit plane for $Re = 428 - 2000$

As observed from the literature, the stability of a flow is dependent on the initial conditions and it is important to avoid background noise and its unwanted forcing effects [Ho and Huerre, 1984]. Due to the inherent nature of experimental work, it is nearly impossible to eliminate background noise and hence, the initial nature of the jet is observed in the frequency space to determine the strength of these disturbances. It is seen in figure 4.4 that no sharp peaks of any substantial magnitude are present and the facility is deemed to be "quiet".

Additionally, the stability of a flow is dependent upon the existence of a laminar boundary layer and hence is an important parameter to be considered. This is done by observing the momentum thickness-Reynolds number relationship. The momentum thickness of the jet is measured by integrating the velocity profile in figure 4.1 from

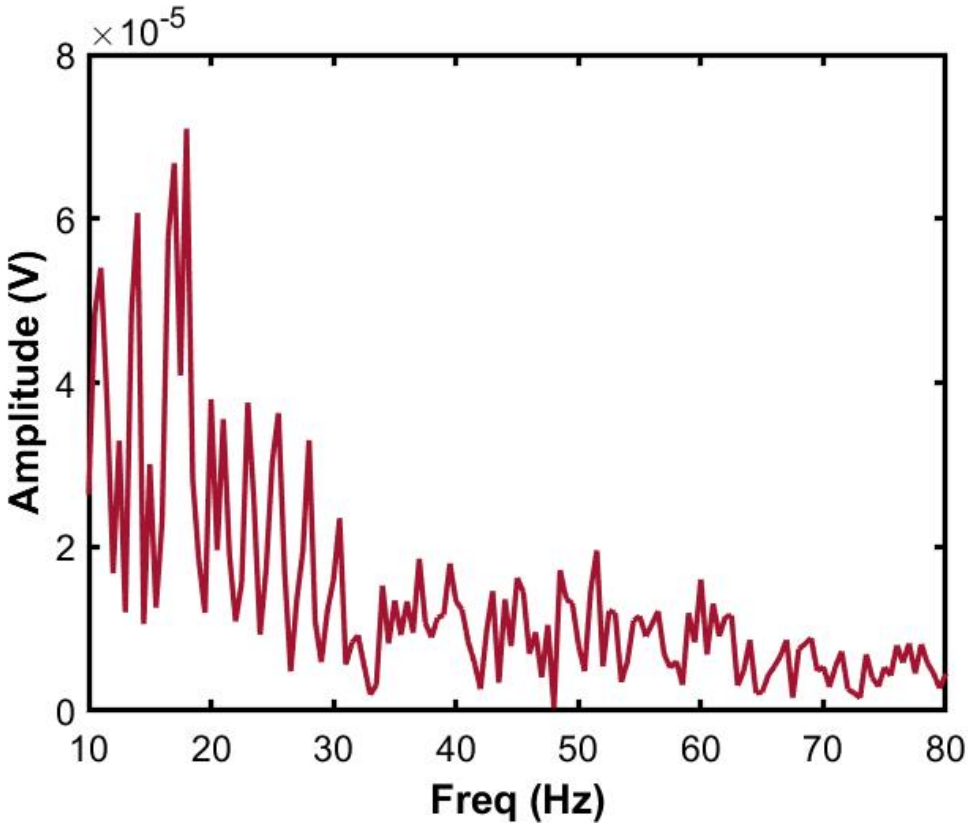

Figure 4.4: Frequency spectrum of the jet for $M = 1$ and $Re = 1680$ at the jet exit plane ($z/D = 0$)

the jet centerline to a specified radial location where the local velocity approaches zero. Mathematically, momentum thickness, θ is calculated by

$$\theta = \int_0^\infty (\frac{u}{U})(1 - \frac{u}{U})dy \tag{4.1}$$

Since hotfilm anemometry relies on the principle of convective cooling, it has an additional constraint of not being accurate in stationary fluids. While measuring the velocity profile beyond the nozzle end walls, the hotfilm probe is responsible for the local heating and motion of the fluid, which is incorrectly measured as the flow field velocity. This effect is more pronounced at lower Reynolds numbers as seen in figure 4.5 and as a consequence, the measured momentum thicknesses are incorrectly larger. This is rectified by truncating the velocity profile at the point where $\frac{u}{U} \to 0.1$.

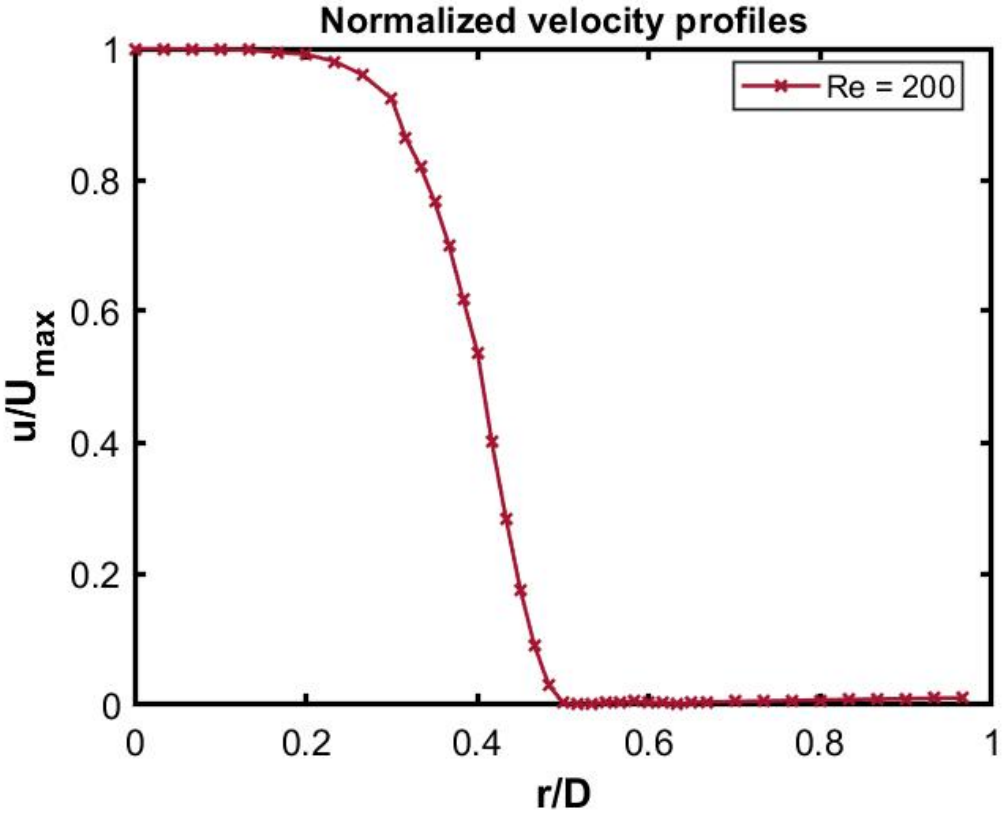

Figure 4.5: Velocity profile for $Re = 200$ and $M = 1$.

A laminar boundary layer is characterized by the inverse relationship between the momentum thickness θ and $\sqrt{Re}$. This linear relationship is seen in figure 4.6.

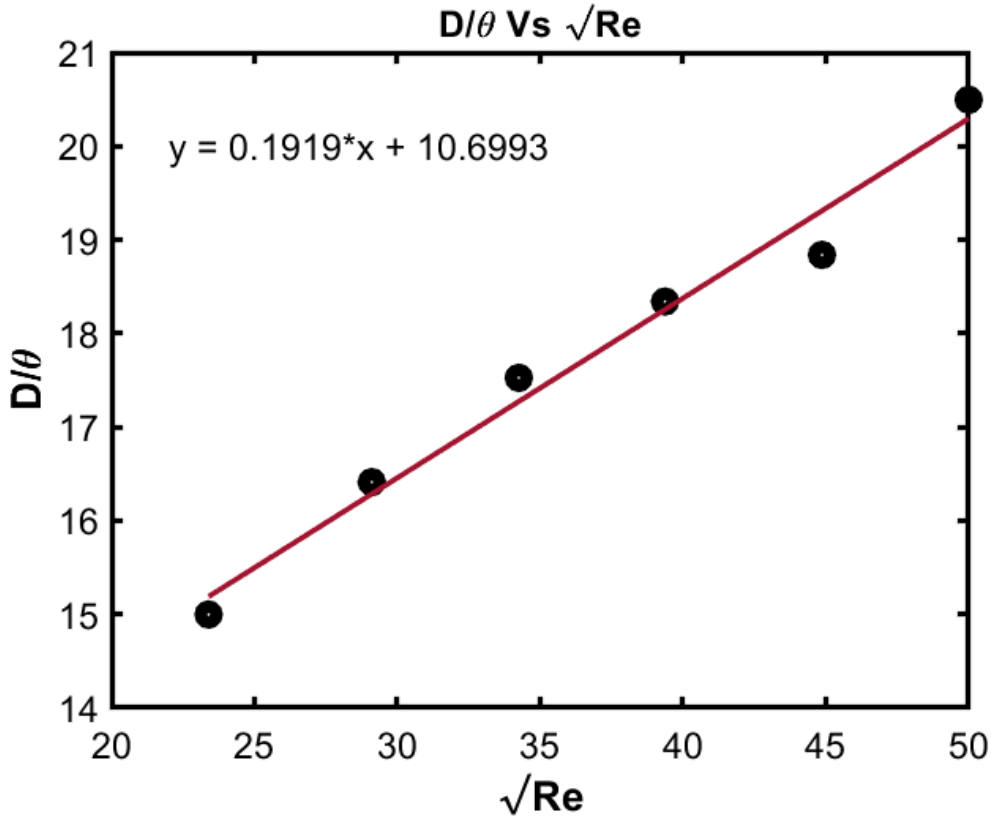

Figure 4.6: Linear relationship between momentum thickness (nondimensionalized) and Reynolds number.

4.2 Flow Visualization Results

After characterizing the jet at $M = 1$, spectral measurements using the hotwire and flow visualization experiments are performed for a range of values, from $M = 45$ to 1. This is repeated for various Reynolds numbers ranging from $Re = 400$ to 3200.

Before hotwire anemometry is carried out, a qualitative analysis of the jet breakup needs to be done through flow visualization. This helps correlate peaks in the frequency space with the jet behavior and helps identify transitional viscosity ratios that ought to be studied deeply.

Figure 4.7 shows the jet breakup at a fixed viscosity ratio (here, $M = 1$) and varying Reynolds numbers, $Re = to$.

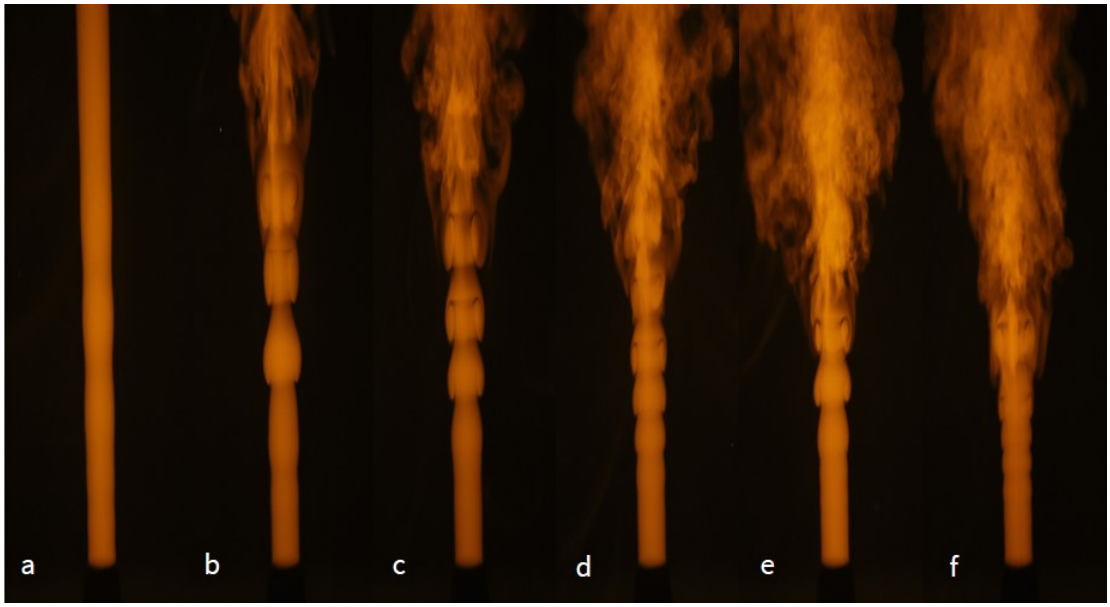

Figure 4.7: Flow visualization of a jet at $M = 1$ for (a) $Re = 428$, (b) $Re = 1040$, (c) $Re = 1545$, (d) $Re = 2009$, (e) $Re = 2540$, and (f) $Re = 3009$

At lower Reynolds numbers, the jet appears to have a long potential core with minimal breakup or mixing, and at increasing Reynolds numbers, "mushroom-like" patterns similar to those observed by D'Olce et al. (2008) become more prominent. The onset of instabilities in the shear layer results in the amplification of perturbations as they travel downstream, and their nonlinear interactions lead to the shear layer rolling up into vortices. Laminar axisymmetric jets produce a vortex street with a frequency dependent on the initial disturbance. Schram [Schram and Hirschberg, 2003] showed how neighboring vortices merge to form a new vortex street with a frequency corresponding to the subharmonic of the initial disturbance frequency. This is illustrated in figure 4.8.

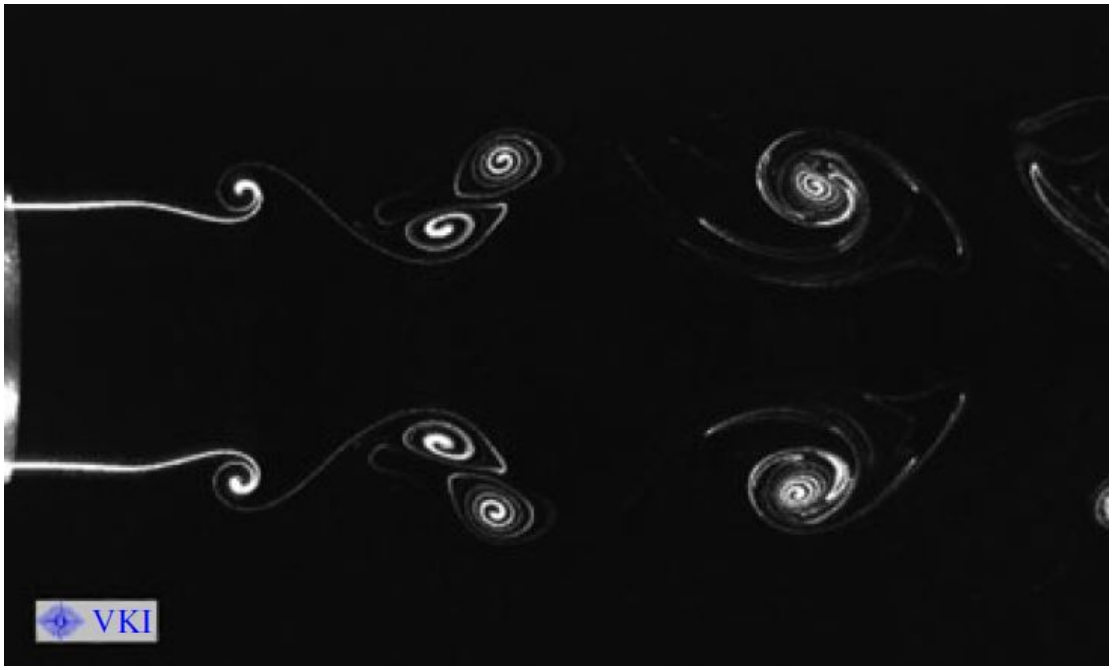

Figure 4.8: Illustration of Vortex pairing in jets (Schram 2003)

The spacing of these vortex rings depends on the magnitude of the initial disturbance and as a consequence, a higher Reynolds number flow produces a larger disturbance that leads to closely spaced vortex rings. These closely spaced vortex rings interact with each other and eventually become unstable and collapse, leading to rapid mixing and break up of the core flow. This is observed in figure 4.7 where the jet breaks up occurs at decreasing distances downstream for increasing Reynolds number.

At a higher viscosity ratio, $M = 45$, for the same range of Reynolds numbers, a combination of the aforementioned axisymmetric mode and a helical mode is observed for $Re = 1332$, shown in figure 4.9. Purely helical modes are observed for $Re > 1676$.

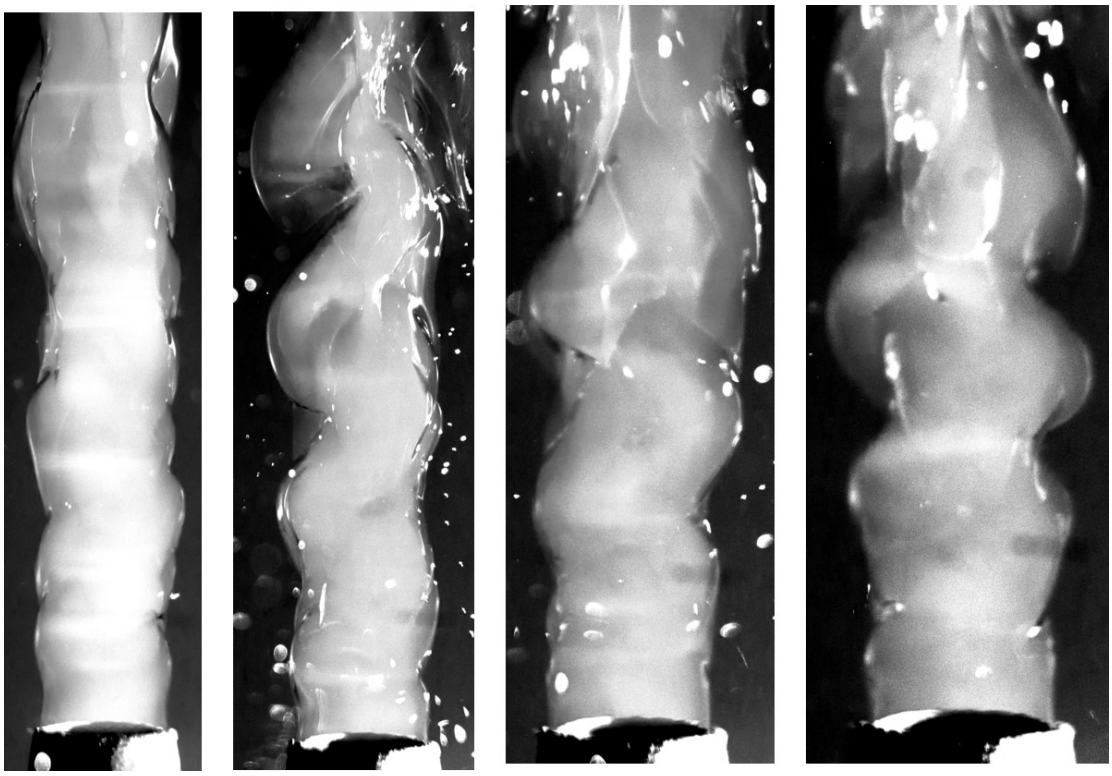

Figure 4.9: Flow visualization of a jet at $M = 45$ for (a) $Re = 1332$, (b) $Re = 1676$, (c) $Re = 2013$, and (d) $Re = 2339$

This interesting dual-mode excitation behavior of the jet is a result of the combination of axial disturbances and nonaxisymmetric helical disturbances at lower frequencies. Helical disturbances are the result of a "wobbling" nozzle or nonaxisymmetric forcing (intrinsic or external) and its effect is to displace successive vortex rings such that they are eccentrically positioned with respect to each other. Such eccentrically placed vortex rings tilt each other in opposite directions, as shown in figure [Parekh et al., 1988] 4.10. These tilted vortex rings move away from each other and stretch the jet core [Reynolds et al., 2003].

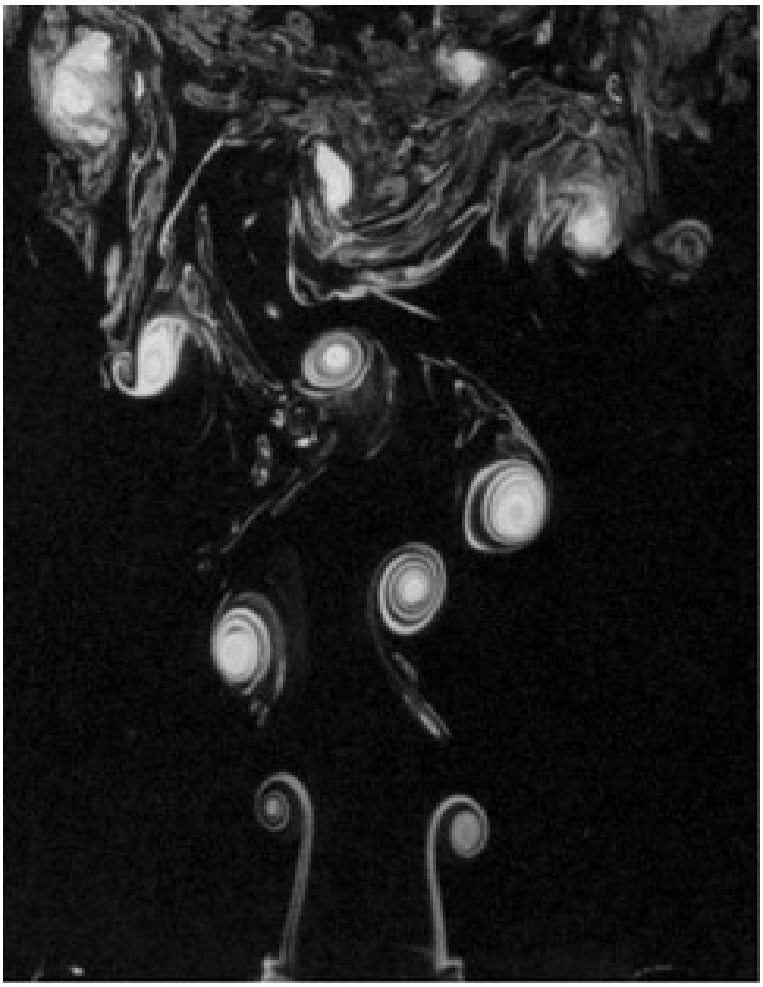

Figure 4.10: Eccentric vortex rings leading to helical mode in a jet [Parekh et al., 1988]

Another interesting phenomenon occurs when the frequency of the helical disturbance is 0.5 of the axisymmetric disturbance frequency. If the perturbation is large enough, the vortex rings will alternately tilt away from each other and the jet is said to bifurcate. Additionally, if the ratio of frequencies is close to half, the jet bifurcates but slowly merges back with each other [Reynolds et al., 2003]. While not conclusive, figure 4.11 shows a small degree of jet bifurcation with at $M \sim 28$ and $Re = 2013$. However, this is not seen at all Reynolds numbers. If the frequency (or Re) is very low, the vortex rings are too far apart to affect each other and the jet undergoes break up.

Alternatively, if the frequency is very high, the vortex rings are too close to each other to separate into two streams. This may explain why this weakly bifurcating jet was only observed in some cases.

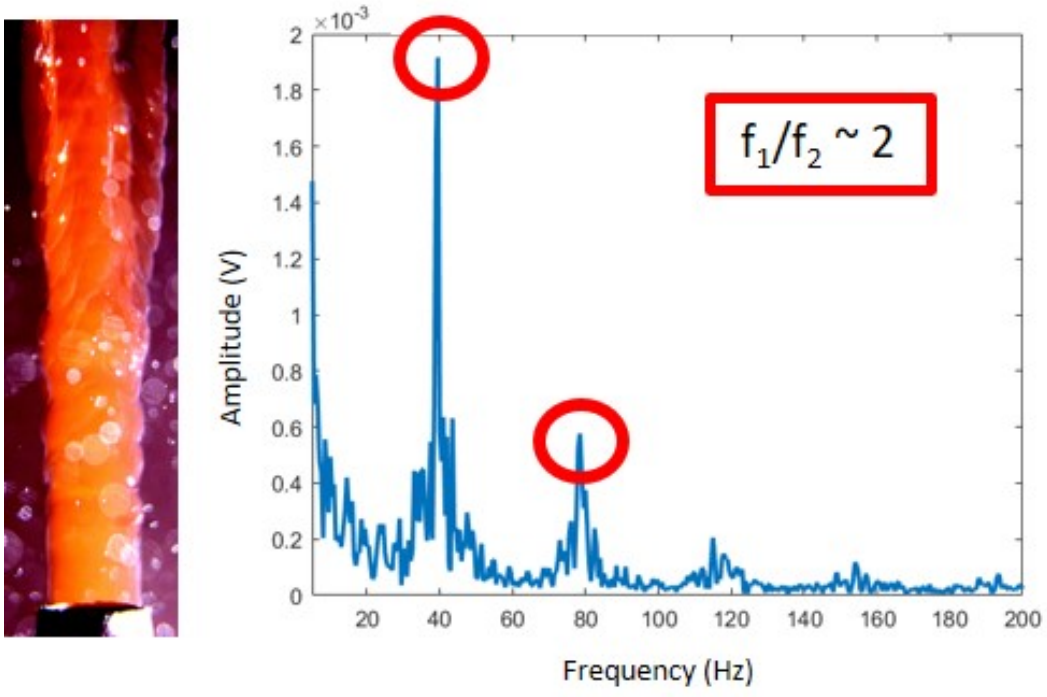

Figure 4.11: *(Left)* Flow visualization of jet at M 28 for $Re = 2013$, *(Right)* Frequency spectrum at $z/D = 1$ for $M = 32$ and Re 2000

Figure 4.12 shows the jet instability at a constant $Re = 2013$ for varying values of viscosity ratios. At $M = 45$, the jet initially displays a helical mode and transitions to an axisymmetric mode with decreasing M. The demarcation between the two modes is not sharp and a combination of the two instabilities is also observed.

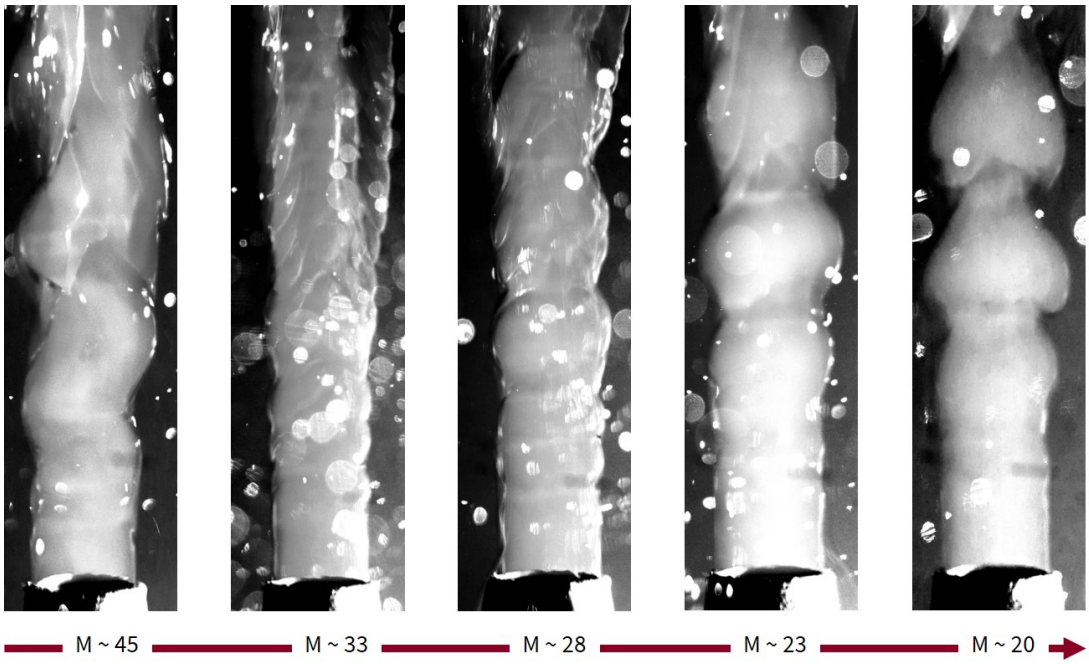

Figure 4.12: Flow visualization of the jet at a constant $Re = 2013$ and varying viscosity ratio ranging from $M = 45$ to 20

For $Re < 1600$, this exact transition is not observed since the jet has a combination of helical and axisymmetric modes at $M = 45$, as shown in figure 4.9 (a). However, lowering the viscosity ratio curbs the helical mode. At low Reynolds numbers ($Re \leq 800$) and high viscosity ratios ($M = 45$), the jet appears to be axisymmetrically unstable initially but folds onto itself and collapses due to its low momentum. Hence, the low Reynolds number case is not studied. Figure (4.13) shows the transitional behavior of the low viscosity jet on the $M - Re$ plane.

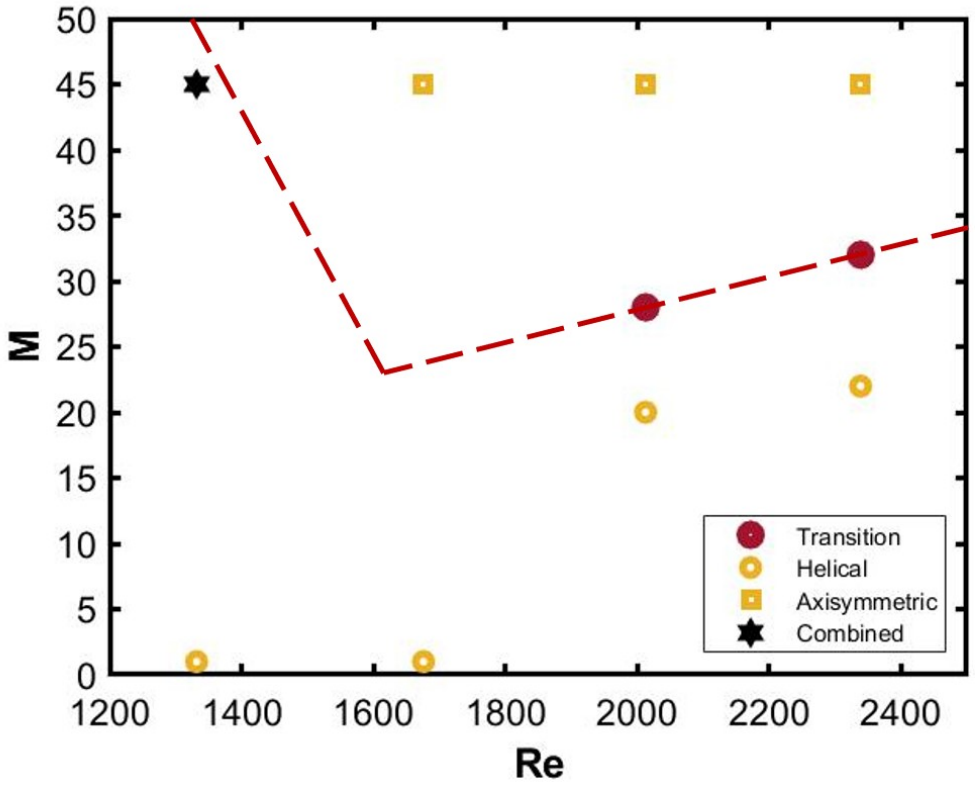

Figure 4.13: Transitional viscosity ratios for jets at varying Re

In summary, it appears that the effect of viscosity is to produce a strong initial helical disturbance for sufficiently high Reynolds numbers, leading to helical modes. The magnitude of axial and helical perturbations might be of the same order for a range of Reynolds numbers where the jet is dually excited.

4.3 Hotwire Anemometry Results

Flow visualization experiments indicate that there is a transition at certain values of M corresponding to a Reynolds number. In order to confirm if this mode transition is associated with the presence of a global mode, spectral characteristics need to be investigated.

Measurements are taken along the centerline and the shear layer at various downstream locations to observe the growth and decay of disturbances. It is noted that the jet is free of disturbances near the nozzle exit ($z/D \to 0$) and the onset of a disturbance is observed at $z/D = 1$. The evolution of these perturbations is captured at $z/D = 2$ and $z/D = 3$ where the peak appears to be the most pronounced. At $z/D = 4$, many peaks appear, leading to a broadband spectrum at $z/D = 5$. Hence, these locations were chosen as the measurement stations for all the cases and depict, fairly well, the growth of a preferred frequency and its subsequent decay due to mixing.

Each measurement is taken at a sampling frequency of 2048 Hz for time, $t = 2$ seconds. This selection allowed for the total time of one trial to stay under 60 seconds. Since the viscosity drops constantly as the jet fluid is issued in the tank, the objective is to finish the trial as quickly as possible to qualify each trial under one viscosity ratio. Viscosity changes at the interface of the jet and the ambient fluid due to mixing and this change is quantified by calculating the diffusion length or the Schmidt number.

The diffusion length is given by $D = \sqrt{Dt}$ where D is the diffusivity of polypropylene glycol into water, $D = 1.23 \times 10^{-5} cm^2/s$ and t is the time taken to complete one trial, $t = 60s$. This results in a diffusion length of about 1% of the jet diameter– small enough to be considered negligible over the course of the trial. Plugging the value of the diffusivity of propylene glycol into the Schmidt number, we get

$$Sc = \frac{\nu}{D} = \frac{\mu}{\rho * D} \tag{4.2}$$

The high Schmidt number,$Sc \approx 813$, indicates that the mass transfer layer is small and hence, mass transfer across the jet core is small compared to momentum effects. If the trial time is increased to improve hotwire fidelity, diffusion processes cannot be neglected accurately.

Hotwire measurements are performed at higher Reynolds numbers since flow visualization indicated an apparent shutoff in axisymmetric-helical transitions. These measurements are taken at equally spaced downstream distances from the jet exit plane and figure 4.14 shows one such case at $Re = 1676$.

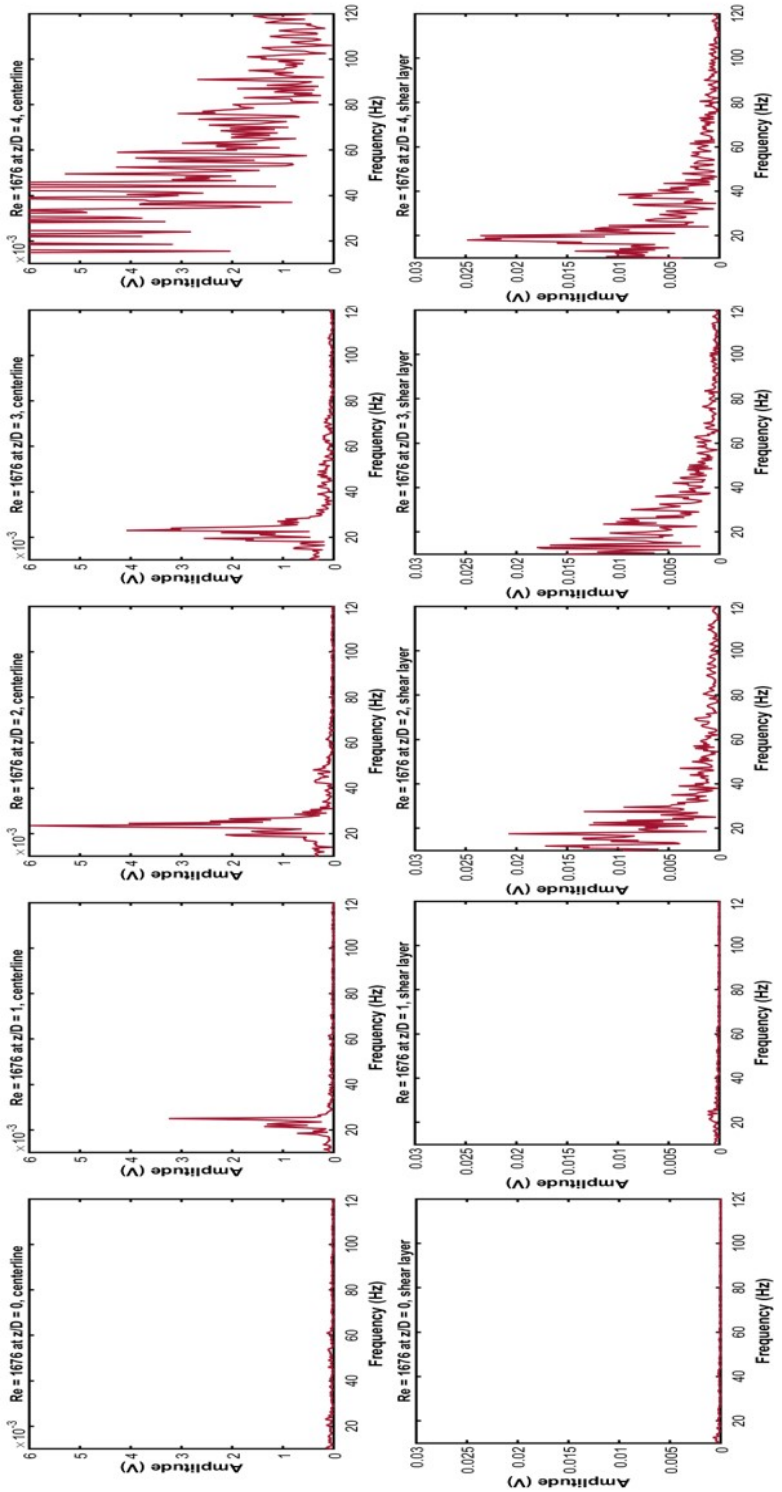

Figure 4.14: Frequency spectrum of the jet at $Re = 1676$ and $M = 45$ along the centerline (*left*) and the shear layer (*right*).

The evolution of a sharp peak from $z/D = 0$ to $z/D = 3$ is clearly seen, after which the jet starts to break up and mix, at $z/D = 4$. The peak frequency is observed to be $f = 23$ Hz. The shear layer is noisier as expected and although a dominant frequency is seen at $z/D = 1 - 2$, a discrete peak is not observed. Figure 4.15 shows the variation of peak frequency in the downstream direction. It is observed that the peak frequency reduces for reducing viscosity ratios at the same z/D location.

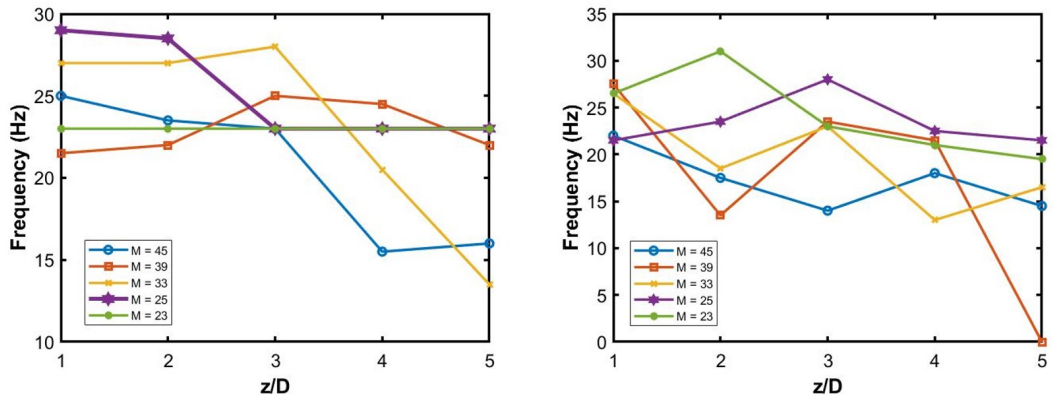

Figure 4.15: Peak frequencies as a function of downstream locations at constant viscosity ratios ($M = 45 - 23$) along the centerline (*left*) and the shear layer (*right*) ($Re = 1676$).

This trend is the same along the centerline and the shear layer. Multiple peaks are seen in the shear layer at downstream locations where the jet mixes, hence making it difficult to determine a single peak. Note that at $M = 23$, the peak frequency remains constant at $f = 23$ Hz even at downstream locations. This behavior is also observed at $M = 25$ where the second dominant peak of comparable magnitude at $z/D = 1$ and $z/D = 2$ is $f = 23$ Hz. Figure 4.16 shows the frequency spectra at far downstream locations where the peak is still clearly observed.

At a constant downstream location, the peak frequencies follow a generally decreasing trend, albeit by a small amount, as shown in figure 4.17

At far away downstream locations, the highest peak in magnitude is chosen amongst the competing frequencies. Therefore, the frequency response of the jet at these locations has a large degree of uncertainty associated with it. Note that the zero peak frequency in figure 4.17 (*right*) corresponds to 'no discrete peak'.

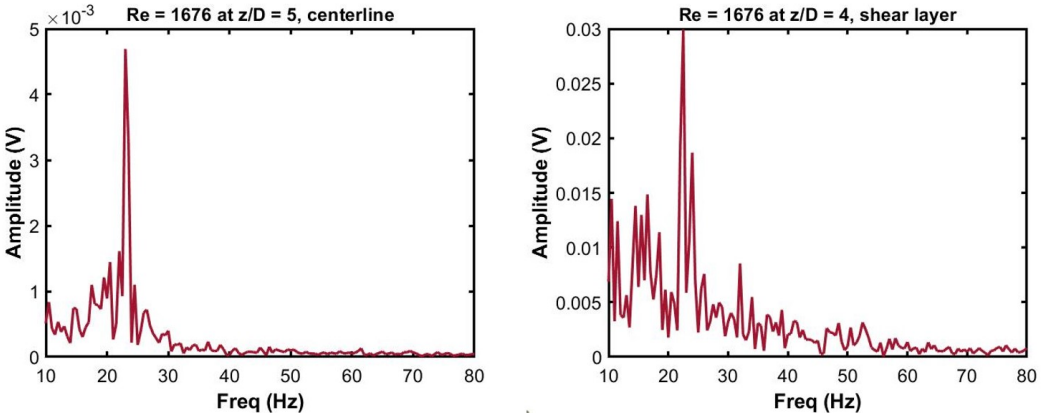

Figure 4.16: Peak frequencies at $z/D = 5$ along the centerline (*left*) and at $z/D = 4$ along the shear layer (*right*) for $M = 25$ ($Re = 1676$).

At lower Reynolds number ($Re = 1339$), the peak frequency was found to be relatively the same for varying viscosity ratio ($M = 45 \rightarrow 20$), as seen in figure 4.18.

Figure 4.19 illustrates the evolution of a dominant frequency from the base state at $z/D = 0$ and its subsequent breakup at $M = 39$ and $Re = 2013$. The magnitude of voltage fluctuation is shown in figure 4.20 and the normalized velocity profiles at various downstream stations are shown in figure 4.21. As expected, centerline fluctuations are much lesser than those in the shear layer.

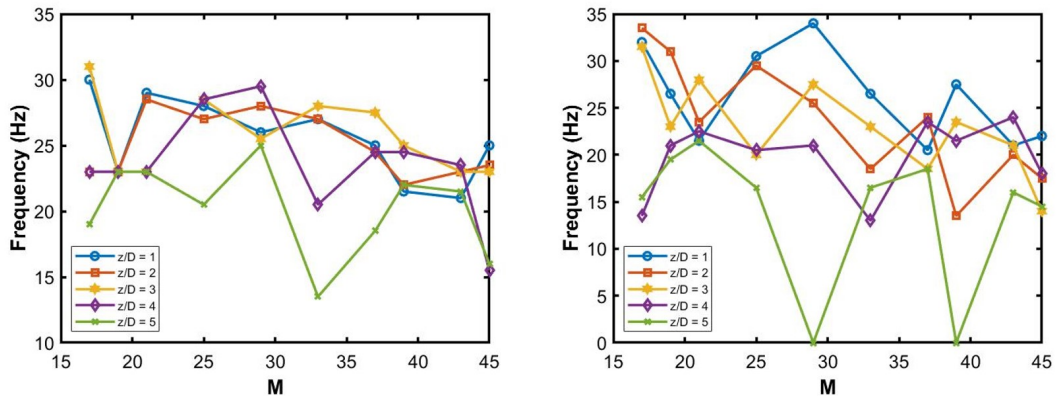

Figure 4.17: Peak frequencies as a function of viscosity ratio at fixed locations downstream ($z/D = 1 - 5$) along the centerline (*left*) and the shear layer (*right*) ($Re = 1676$).

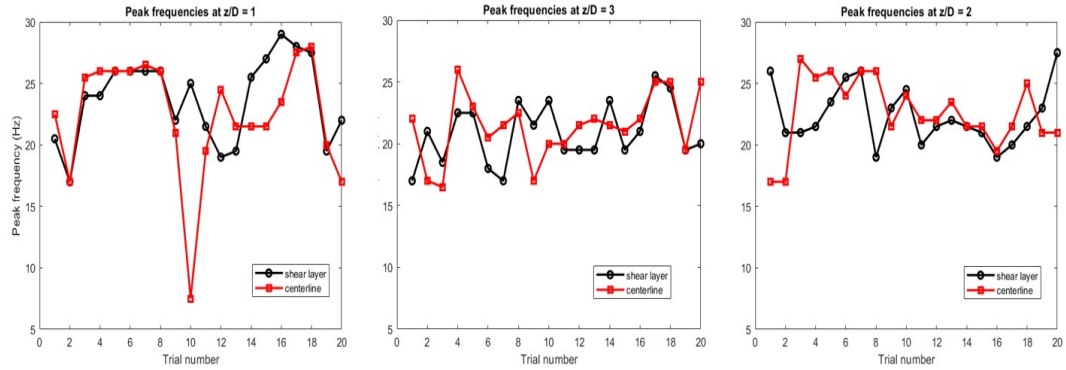

Figure 4.18: Peak frequencies as a function of viscosity ratio at fixed locations downstream ($z/D = 1 - 3$) along the centerline and the shear layer ($Re = 1339$). Increasing trial number denotes decreasing viscosity ratios from $M = 45$ to $M = 20$.

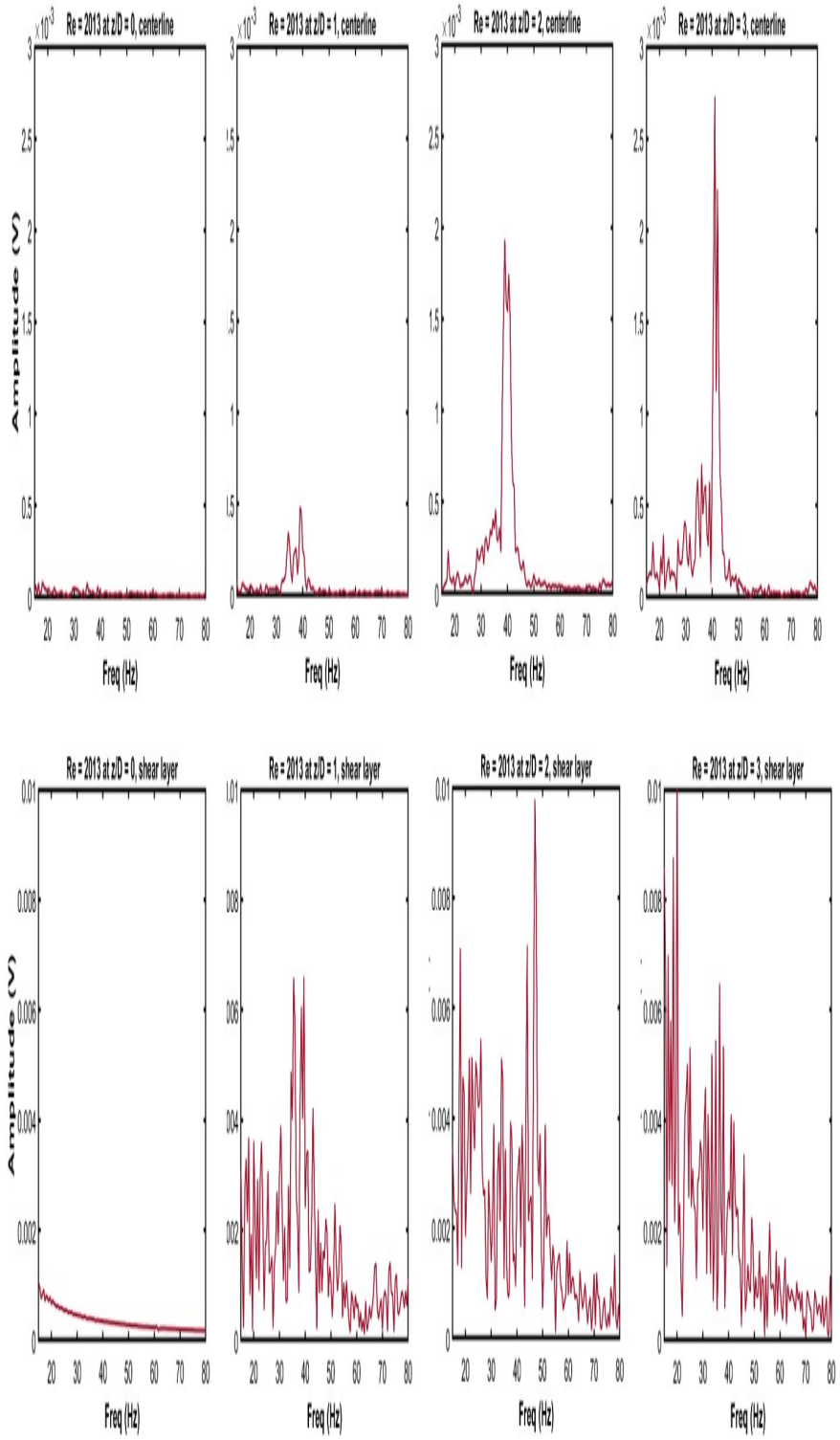

Figure 4.19: Evolution of the dominant frequency in the frequency spectrum along the centerline (*left*) and the shear layer (*right*) for $M = 39$ ($Re = 2013$).

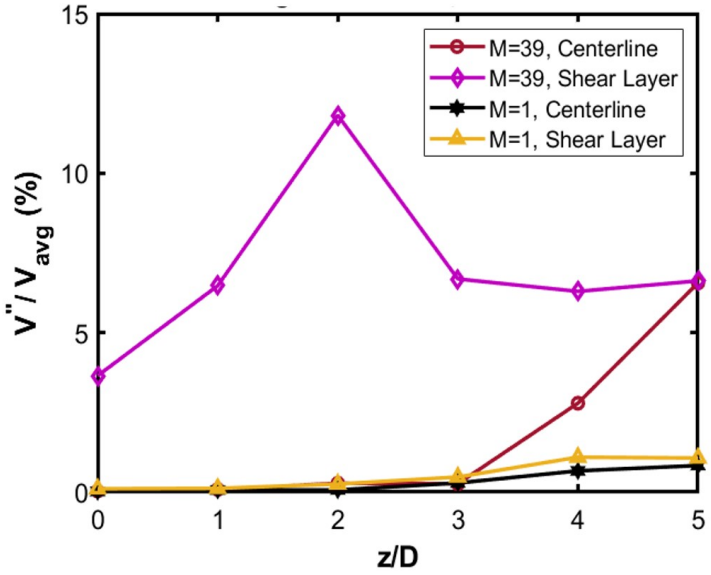

Figure 4.20: Magnitude of measured voltage fluctuation in the jet centerline and shear layer for $M = 39$ ($Re = 2013$).

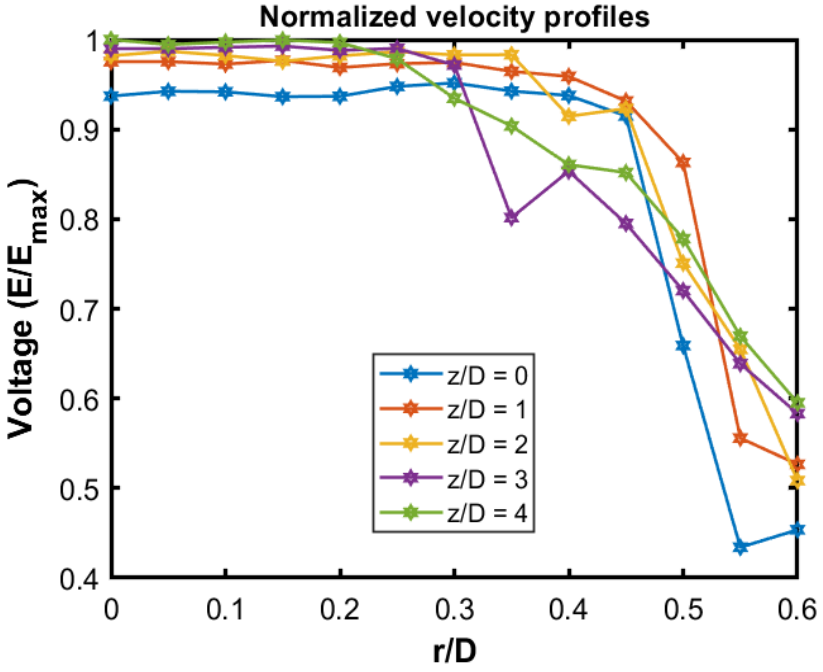

Figure 4.21: Velocity measurements of a viscous jet at various locations downstream ($z/D = 0 - 4$) for $M = 28$ ($Re = 2013$).

Figure 4.22, figure 4.23, figure 4.24, and figure 4.25 show the frequency spectrum of the jet breakup at ($Re = 2332$, $M = 32$), ($Re = 2669$, $M = 38$), ($Re = 3016$, $M = 45$), and ($Re = 3349$, $M = 45$) respectively.

The signal gets noisier as Re increases due to rapid mixing. A discrete peak is lost and a broadbrand spectrum appears. Figures 4.26, 4.27, 4.28 show the peak frequency as a function of downstream location and viscosity ratio for $Re = 2669$, $Re = 3016$, and $Re = 3349$ respectively.

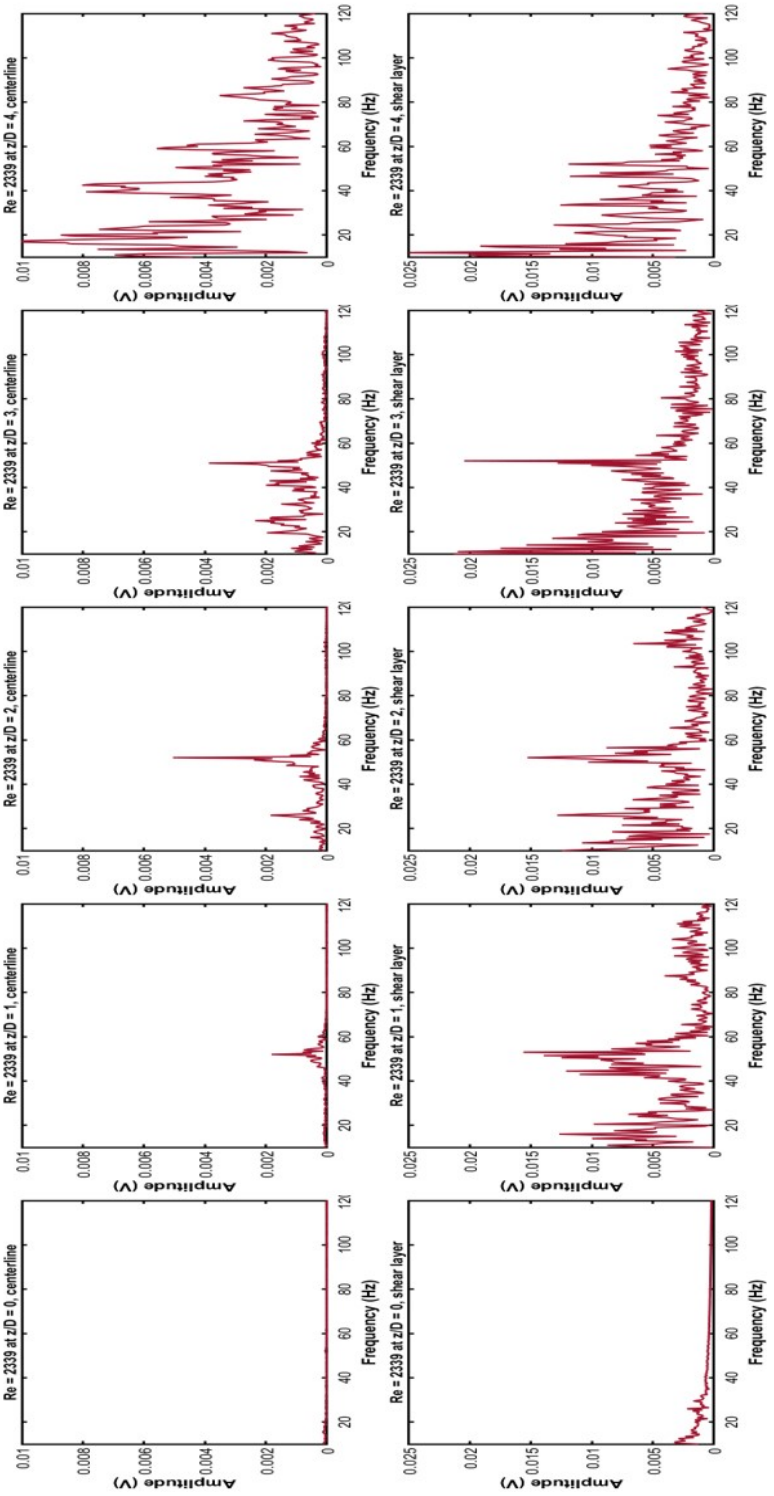

Figure 4.22: Evolution of the dominant frequency in the frequency spectrum along the centerline (*left*) and the shear layer (*right*) for $M = 32$ ($Re = 2332$).

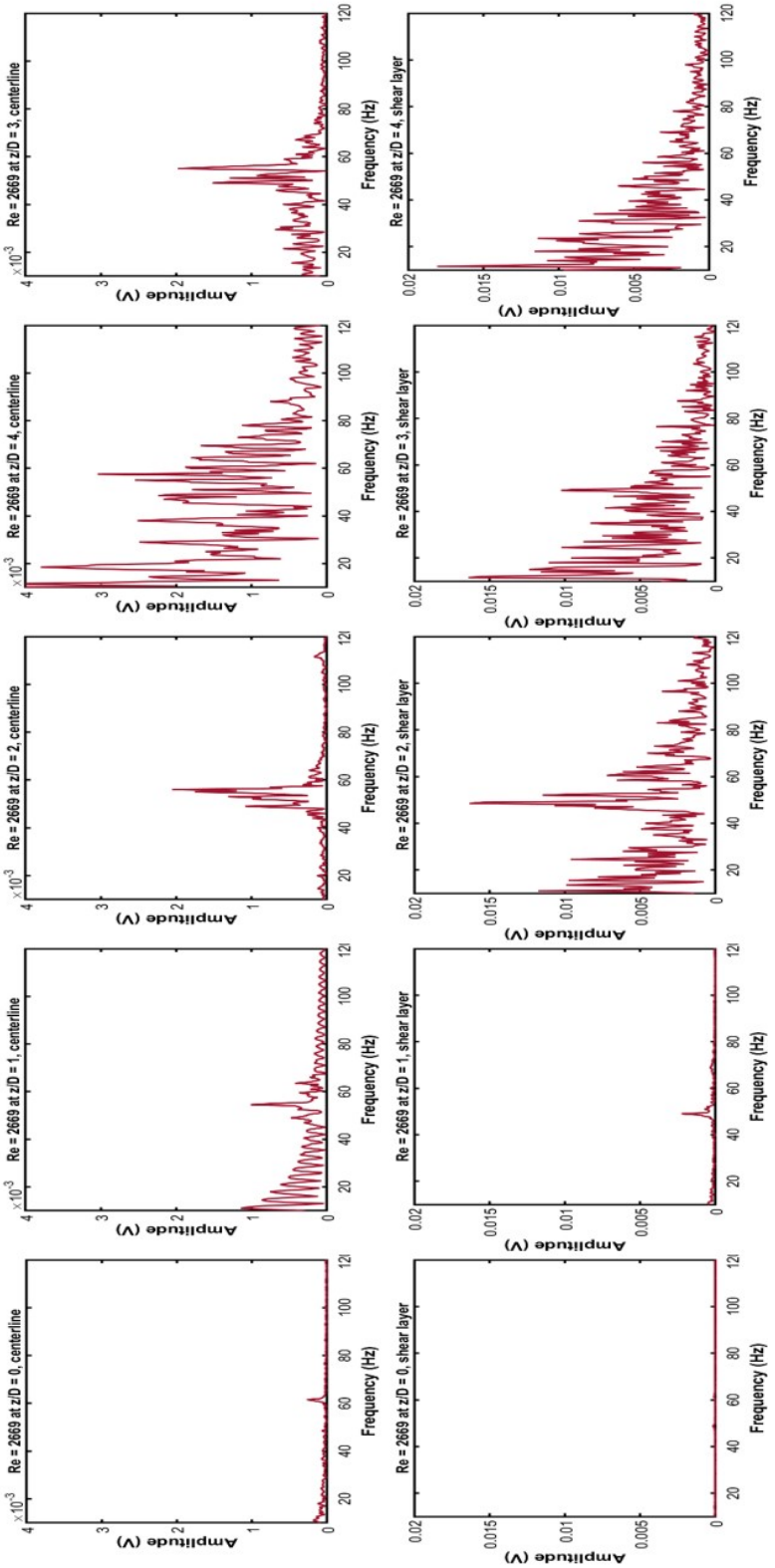

Figure 4.23: Evolution of the dominant frequency in the frequency spectrum along the centerline (*left*) and the shear layer (*right*) for $M = 38$ ($Re = 2669$).

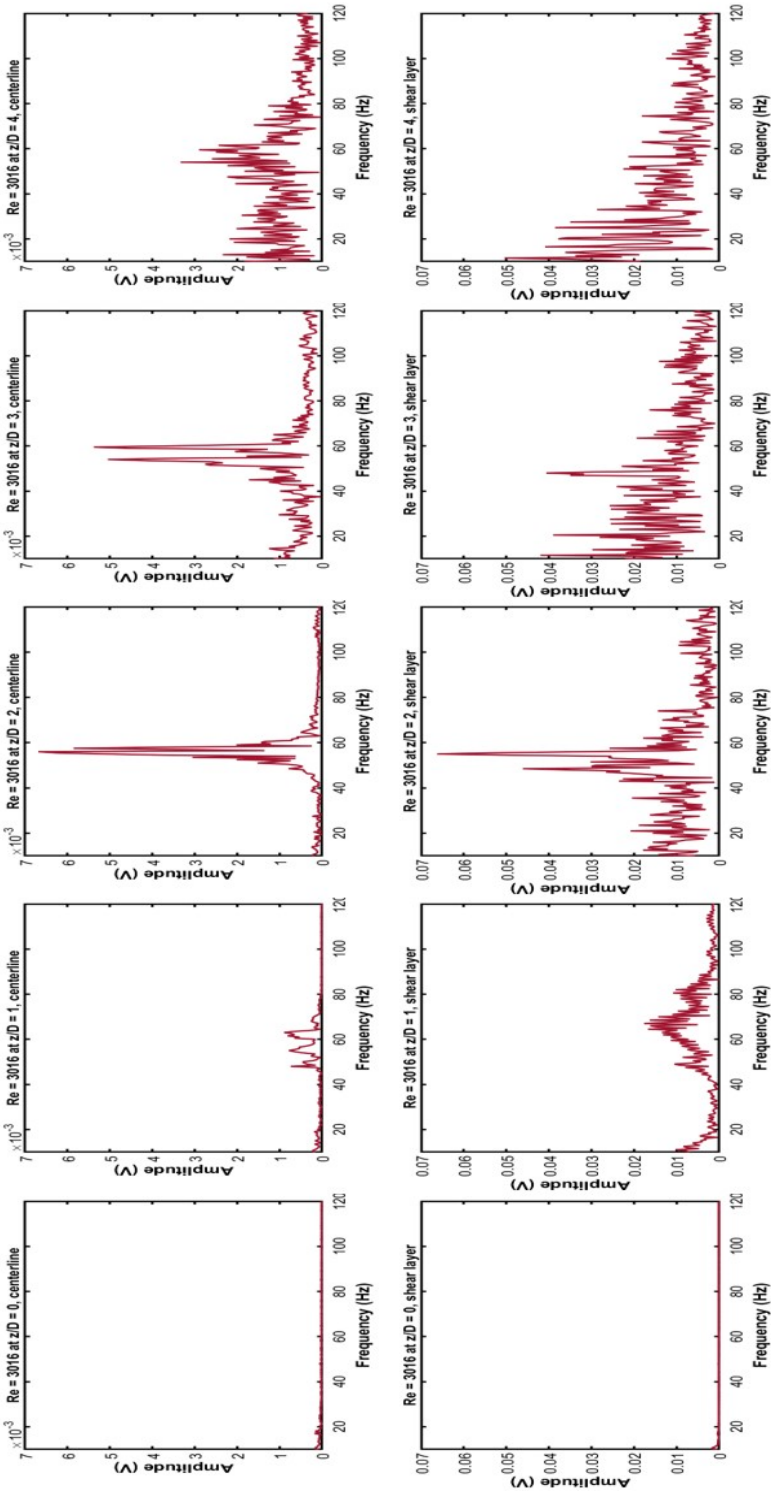

Figure 4.24: Evolution of the dominant frequency in the frequency spectrum along the centerline (*left*) and the shear layer (*right*) for $M = 45$ ($Re = 3016$).

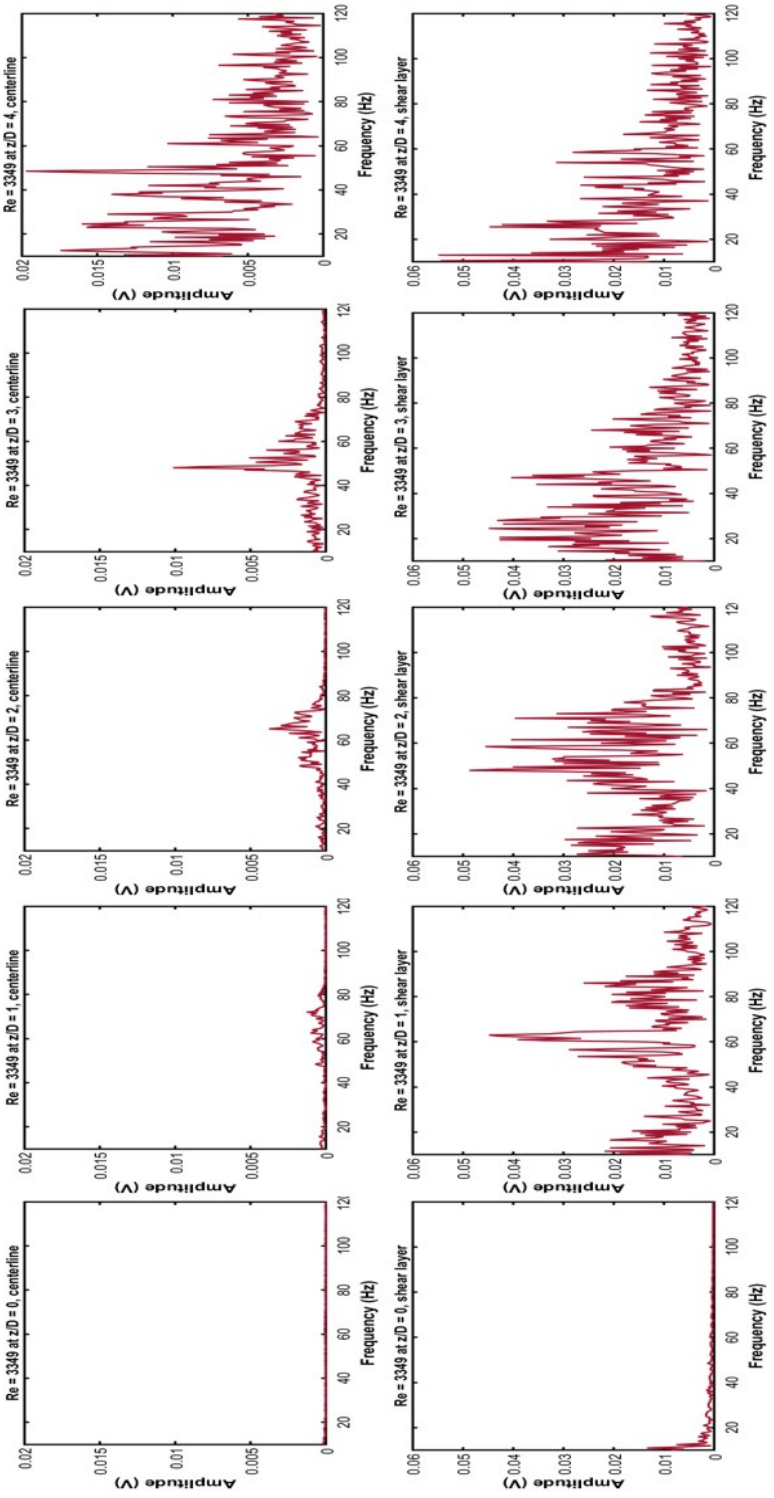

Figure 4.25: Evolution of the dominant frequency in the frequency spectrum along the centerline (*left*) and the shear layer (*right*) for $M = 45$ ($Re = 3349$).

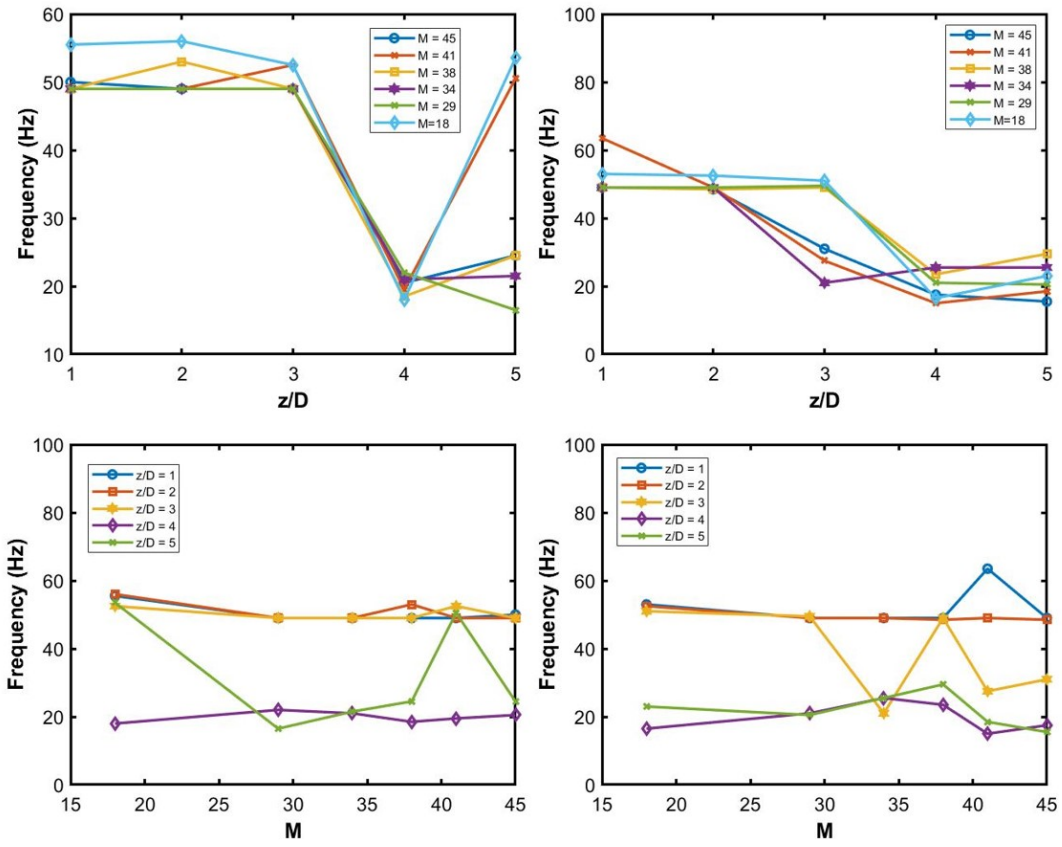

Figure 4.26: Peak frequencies as a function of viscosity ratios at fixed locations downstream (*top row*) and as a function of downstream locations at fixed M (*bottom row*) along the centerline (*left column*) and the shear layer (*right column*) ($Re = 2669$).

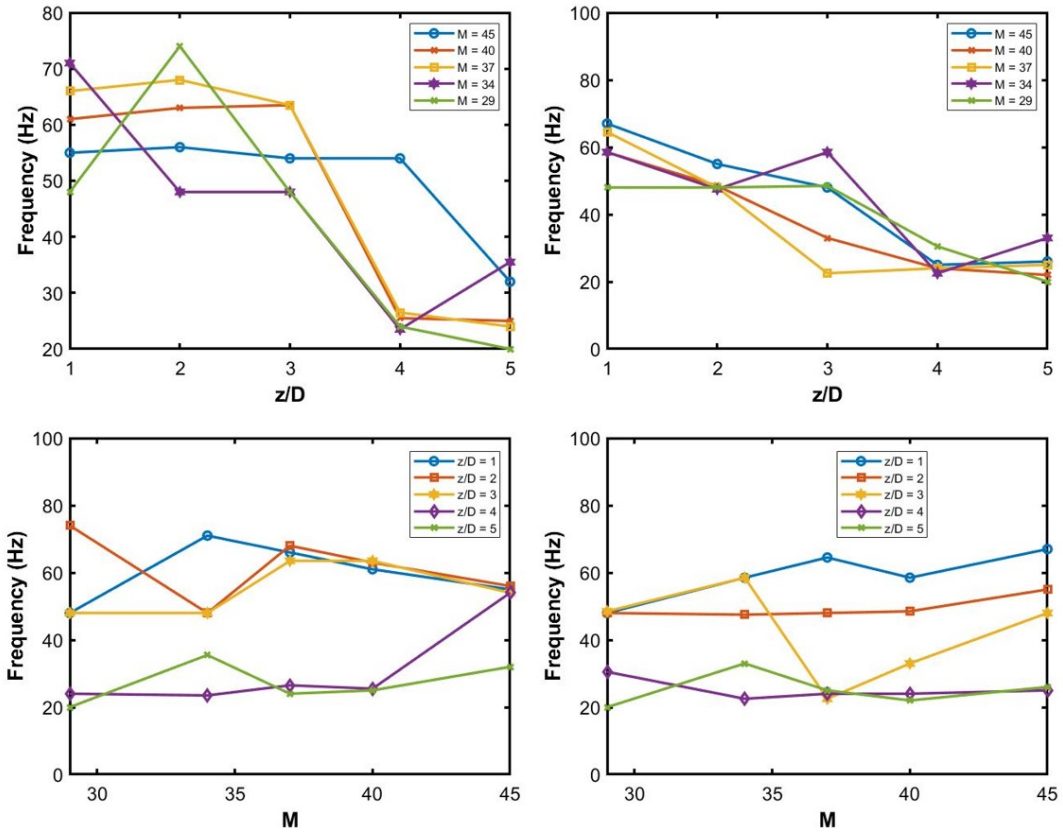

Figure 4.27: Peak frequencies as a function of viscosity ratios at fixed locations downstream (*top row*) and as a function of downstream locations at fixed M (*bottom row*) along the centerline (*left column*) and the shear layer (*right column*) ($Re = 3016$).

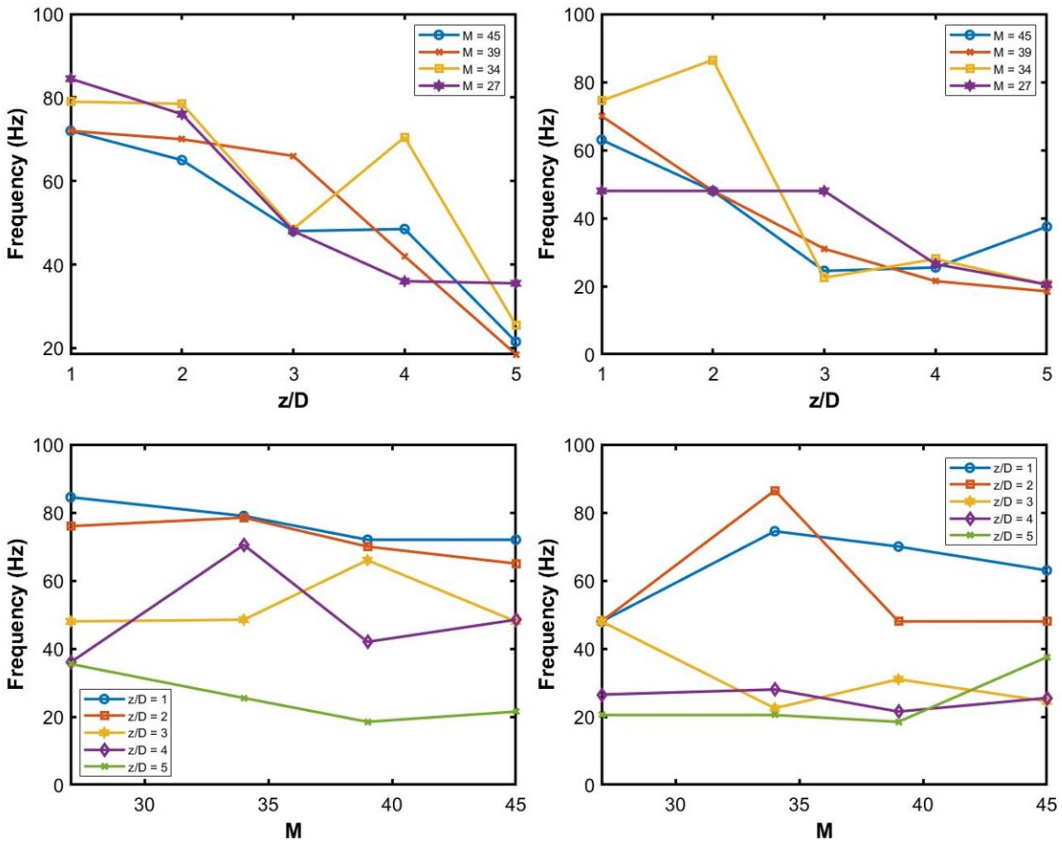

Figure 4.28: Peak frequencies as a function of viscosity ratios at fixed locations downstream (*top row*) and as a function of downstream locations at fixed M (*bottom row*) along the centerline (*left column*) and the shear layer (*right column*) ($Re = 3349$).

As more saltwater is added into the ambient tank via the jet, the viscosity of the tank decreases. However, due to molecular interactions, the density of the ambient fluid also increases despite both the fluids being density matched initially.

The effects of this density difference are quantified through the Richardson number, which is the ratio of buoyant effects to shear effects and is expressed as

$$Ri = \frac{g\delta\rho D}{\rho V^2} \tag{4.3}$$

where g is the acceleration due to gravity, $\delta\rho$ is the density difference, D is the characteristic length (jet diameter here), and V is the velocity of the incoming jet. At the lowest Reynolds number, $Re = 1676$ (or the lowest V), and the lowest viscosity ratio, (highest density difference, $\delta\rho = 0.010\ kg/m^3$), the Richardson number is calculated to be $Ri = 0.0728$. In other words, the buoyant effects are 7.2% as important as the shear effects. Figure 4.29 shows the relative importance of buoyant effects compared to shear effects and since the region of interest lies at a higher Re and viscosity ratios, the density difference is not very large at these points. This means that buoyant effects can be considered negligible.

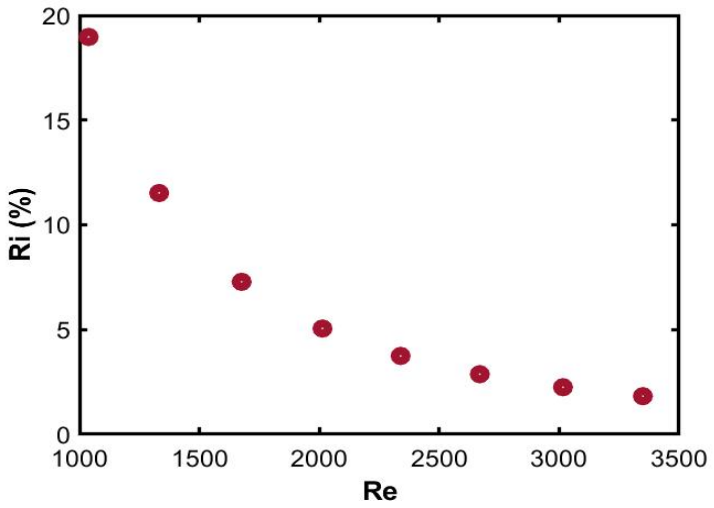

Figure 4.29: Variation of Richardson number, Ri, for increasing Re at the lowest viscosity ratio ($\delta\rho = 0.010\ kg/m^3$)

4.4 External Forcing

Global modes are relatively insensitive to external forcing within a certain range [Hallberg and Strykowski, 2008] and this characteristic can, in turn, be used to identify global modes.

A pure sine wave was used to force the base jet flow using external speakers. The speaker is directed towards the jet and hotwire measurements are taken at a constant Reynolds number for varying strengths of external forcing. The frequency of the sine wave used to excite the flow is selected based on the preferred frequency of the jet.

Figure (4.30) shows an example case of a jet at $Re = 1330$ and $M = 1$ being acoustically forced by a pure tone of $f = 27$Hz of 75.9 dB strength. It is evident that the forcing frequency overrides the intrinsic dynamics of the flow and appears as the dominant frequency and hence, no useful information is obtained from this experiment.

It has to be noted that the fluid at the jet exit plane must be forced, but the configuration of speakers used in this study are placed next to the test section wall facing the nozzle. This results in forcing the entire domain where perturbations grow and decay, and hence this technique is flawed.

Figure 4.31 shows the spectral characteristics of a jet at $M = 45$ with the acoustic exciter placed near the overhead reservoir. The externally applied frequency of $35Hz$ is absent in the spectrum. This is possibly due to the effects of plumbing, rotameter, valves, honeycomb flow straightener, and diffuser connecting the overhead reservoir to the test section through which the fluid has to pass.

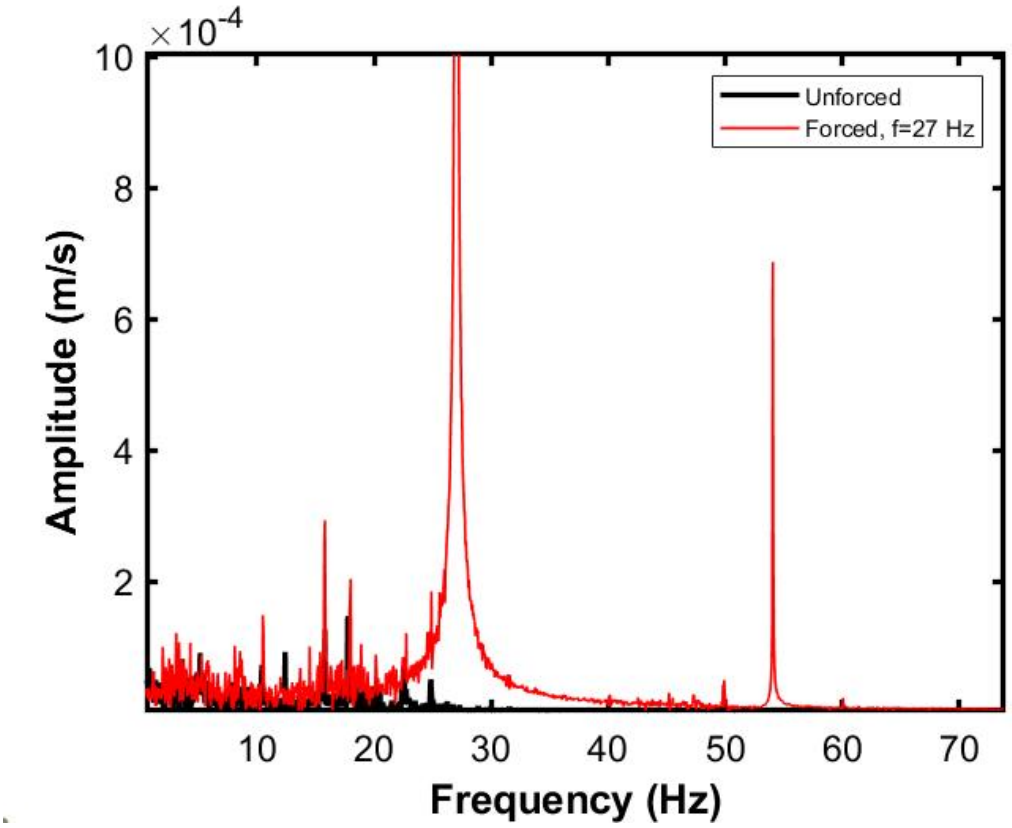

Figure 4.30: Acoustically forced jet by a forcing frequency of $f = 27$ Hz, at$M = 1$ and $Re = 1330$. The strength of the external frequency is 75.9 dB

In the current setup, it is not possible to place the acoustic exciter under the test section, facing the diffuser, because the speaker induces structural vibrations that contaminate the entire domain. A modification in the test facility or a directional acoustic exciter is necessary to perform this study in the future.

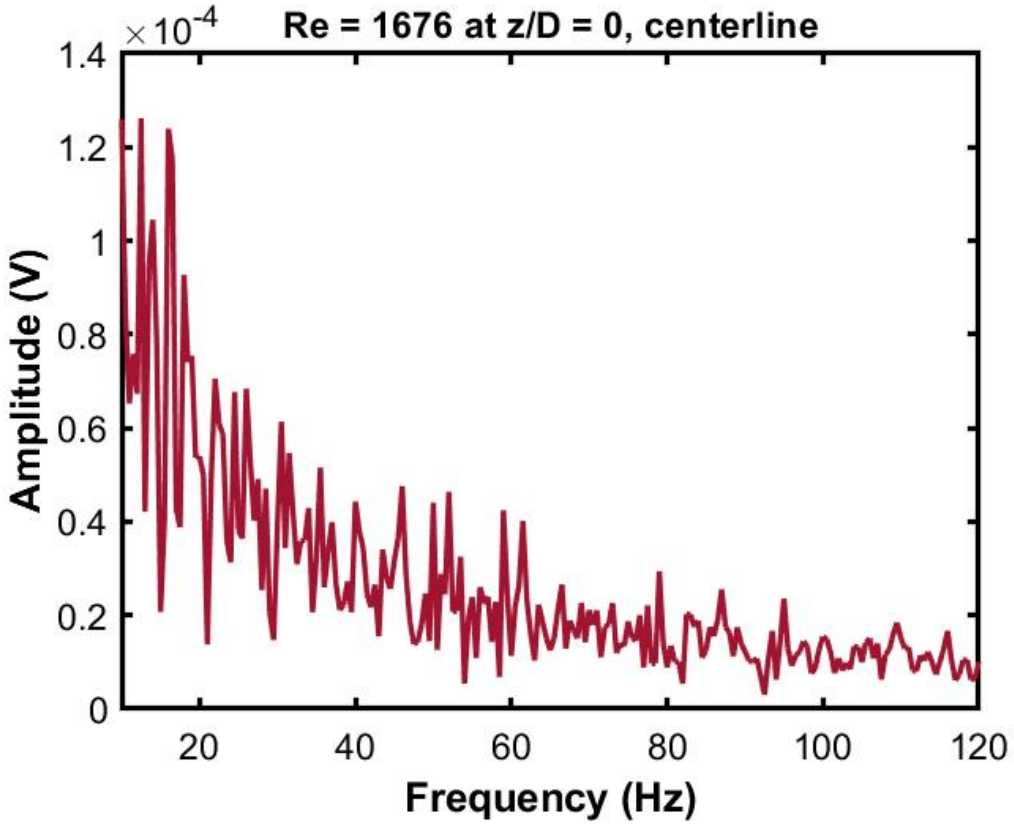

Figure 4.31: Acoustically forced jet by a forcing frequency of f = Hz, at$M = 45$ and $Re = 1676$. The acoustic exciter is placed near the overhead reservoir

Chapter 5

Conclusion

The role of viscosity on the jet breakup is studied at different viscosity ratios and Reynolds numbers. A laminar low viscosity jet is issued into a viscous ambient and the evolution of instabilities is studied using hotwire anemometry and flow visualization. The viscosity ratio is varied from $M = 1$ to 45 and the Reynolds number is varied from $Re = 1300 - 3200$.

In order to capture the dominant frequency of the jet, a hotfilm probe is used at 5 different downstream locations, both along the centerline and the shear layer. Sharp peaks are observed at small downstream distances and a more broadband distribution is observed farther away indicating mixing. Flow visualization is performed using a fluorescent dye (Rhodamine B) and high-speed photography.

For higher Reynolds numbers ($Re > 1600$), helical modes are observed in the jet for high viscosity ratios. When salt water is added, the viscosity ratio drops, and a transition from helical mode to axisymmetric mode is observed. At lower Reynolds numbers ($Re < 1600$), it appears that the jet exhibits both the modes, and hence, a clear transition is not observed. Flow visualization also reveals a weak bifurcation of the jet observed at certain combinations of M and Re.

Spectral analysis of these transitional points reveals a sharp peak at a certain frequency, but this peak disappears further downstream where jet breakup occurs. This peak frequency is a function of both Re and M. The peak frequency increases as Re increases and decreases when M is reduced at a particular location. At $Re = 1676$, it appears that for a region of viscosity ratios, the discrete peak frequency does not

change as a function of the downstream location. This persisting frequency even at the jet breakup regime may be an indication of the existence of a global mode.

Although forcing studies are carried out, the amplitude of the forcing frequency is much higher than the amplitude of disturbances in the base state ($f_{forcing}/f_n \approx 76$) and hence, this study does not yield any fruitful results.

Discrete peaks in the frequency spectra and axisymmetric-helical mode transitions indicate a possible existence of global modes. However, further studies targeting the response of the observed modes to external excitations are crucial in determining if this truly is a global mode. Integrating PIV technique to visualize the flow will substantially improve the current understanding of actual velocity profiles and the formation of structures in viscous jets. Alternatively, a different combination of fluids that result in a higher viscosity ratio may be required to visualize the mode transition for lower Reynolds numbers. Replacing the ambient fluid with a counterflowing one may work to increase the shear rates and possibly lead to global modes. Using multiple hotfilm probes located far away from each other along the centerline/shear layer can help accurately capture the evolution of disturbances while allowing for better control of the viscosity ratio.

References

[Aul and Olbricht, 1990] Aul, R. W. and Olbricht, W. L. (1990). Stability of a thin annular film in pressure-driven, low-reynolds-number flow through a capillary. *Journal of Fluid Mechanics*, 215:585–599.

[Barthelet et al., 1995] Barthelet, P., Charru, F., and Fabre, J. (1995). Experimental study of interfacial long waves in a two-layer shear flow. *Journal of Fluid Mechanics*, 303:23–53.

[Berger and Wille, 1972] Berger, E. and Wille, R. (1972). Periodic flow phenomena. *Annual Review of Fluid Mechanics*, 4(1):313–340.

[Bogey and Bailly, 2010] Bogey, C. and Bailly, C. (2010). Influence of nozzle-exit boundary-layer conditions on the flow and acoustic fields of initially laminar jets. *Journal of Fluid Mechanics*, 663:507–538.

[Cao et al., 2003] Cao, Q., Ventresca, A. L., Sreenivas, K. R., and Prasad, A. K. (2003). Instability due to viscosity stratification downstream of a centerline injector. *The Canadian Journal of Chemical Engineering*, 81(5):913–922.

[Charles and Lilleleht, 1965] Charles, M. E. and Lilleleht, L. U. (1965). An experimental investigation of stability and interfacial waves in co-current flow of two liquids. *Journal of Fluid Mechanics*, 22(2):217–224.

[Charru and Hinch, 2000] Charru, F. and Hinch, E. J. (2000). 'phase diagram' of interfacial instabilities in a two-layer couette flow and mechanism of the long-wave instability. *Journal of Fluid Mechanics*, 414:195–223.

[Chomaz et al., 1991] Chomaz, J.-M., Huerre, P., and Redekopp, L. G. (1991). A frequency selection criterion in spatially developing flows. *Studies in Applied Mathematics*, 84(2):119–144.

[Craik, 1969] Craik, A. D. D. (1969). The stability of plane couette flow with viscosity stratification. *Journal of Fluid Mechanics*, 36(4):685–693.

[Crow and Champagne, 1971] Crow, S. C. and Champagne, F. H. (1971). Orderly structure in jet turbulence. *Journal of Fluid Mechanics*, 48(3):547–591.

[d'Olce et al., 2009] d'Olce, M., MARTIN, J., RAKOTOMALALA, N., SALIN, D., and TALON, L. (2009). Convective/absolute instability in miscible core-annular flow. part 1: Experiments. *Journal of Fluid Mechanics*, 618:305–322.

[Drazin and Reid, 1981] Drazin, P. and Reid, W. (1981). *Hydrodynamic Stability*. Cambridge Monographs on Mechanics. Cambridge University Press.

[Drazin, 2002] Drazin, P. G. (2002). *Introduction to Hydrodynamic Stability*. Cambridge Texts in Applied Mathematics. Cambridge University Press.

[d'Olce et al., 2008] d'Olce, M., Martin, J., Rakotomalala, N., Salin, D., and Talon, L. (2008). Pearl and mushroom instability patterns in two miscible fluids' core annular flows. *Physics of Fluids*, 20(2):024104.

[Fjørtoft, 1950] Fjørtoft, R. (1950). *Application of Integral Theorems in Deriving Criteria of Stability for Laminar Flows and for the Baroclinic Circular Vortex, Etc.* [Geofysiske publikasjoner. vol. 17. no. 6.]. Oslo.

[Govindarajan, 2004] Govindarajan, R. (2004). Effect of miscibility on the linear instability of two-fluid channel flow. *International Journal of Multiphase Flow*, 30(10):1177–1192.

[Govindarajan and Sahu, 2014] Govindarajan, R. and Sahu, K. C. (2014). Instabilities in viscosity-stratified flow. *Annual Review of Fluid Mechanics*, 46(1):331–353.

[Gutmark and Ho, 1983] Gutmark, E. and Ho, C. (1983). Preferred modes and the spreading rates of jets. *The Physics of Fluids*, 26(10):2932–2938.

[Hallberg and Strykowski, 2006] Hallberg, M. P. and Strykowski, P. J. (2006). On the universality of global modes in low-density axisymmetric jets. *Journal of Fluid Mechanics*, 569:493–507.

[Hallberg and Strykowski, 2008] Hallberg, M. P. and Strykowski, P. J. (2008). Open-loop control of fully nonlinear self-excited oscillations. *Physics of Fluids*, 20(4):041703.

[Ho and Huerre, 1984] Ho, C. and Huerre, P. (1984). Perturbed free shear layers. *Annual Review of Fluid Mechanics*, 16(1):365–422.

[Ho and Huang, 1982] Ho, C.-M. and Huang, L.-S. (1982). Subharmonics and vortex merging in mixing layers. *Journal of Fluid Mechanics*, 119:443–473.

[Hu and Joseph, 1989] Hu, H. H. and Joseph, D. D. (1989). Lubricated pipelining: stability of core-annular flow. part 2. *Journal of Fluid Mechanics*, 205:359–396.

[Huerre and Monkewitz, 1990] Huerre, P. and Monkewitz, P. A. (1990). Local and global instabilities in spatially developing flows. *Annual Review of Fluid Mechanics*, 22:473–537.

[Jendoubi and Strykowski, 1994] Jendoubi, S. and Strykowski, P. J. (1994). Absolute and convective instability of axisymmetric jets with external flow. *Physics of Fluids*, 6(9):3000–3009.

[Joseph, 1976] Joseph, D. (1976). *Stability of Fluid Motions*. Number v. 1 in Springer tracts in natural philosophy. Springer-Verlag.

[Kao and Park, 1972] Kao, T. W. and Park, C. (1972). Experimental investigations of the stability of channel flows. part 2. two-layered co-current flow in a rectangular channel. *Journal of Fluid Mechanics*, 52(3):401–423.

[Koch, 1985] Koch, W. (1985). Local instability characteristics and frequency determination of self-excited wake flows. *Journal of Sound and Vibration*, 99(1):53–83.

[Kouris and Tsamopoulos, 2002] Kouris, C. and Tsamopoulos, J. (2002). Dynamics of the axisymmetric core-annular flow. ii. the less viscous fluid in the core, saw tooth waves. *Physics of Fluids*, 14(3):1011–1029.

[Kundu et al., 2012] Kundu, P. K., Cohen, I. M., and Dowling, D. R. (2012). Chapter 11 - instability. In *Fluid Mechanics (Fifth Edition)*, pages 473–540. Academic Press, Boston, fifth edition edition.

[Kyle and Sreenivasan, 1993] Kyle, D. M. and Sreenivasan, K. R. (1993). The instability and breakdown of a round variable-density jet. *Journal of Fluid Mechanics*, 249:619–664.

[Landau and Lifshitz, 1959] Landau, L. D. and Lifshitz, E. M. (1959). *Fluid mechanics*.

[Lecordier et al., 1991] Lecordier, J. C., Hamma, L., and Paranthoen, P. (1991). The control of vortex shedding behind heated circular cylinders at low reynolds numbers. *Experiments in Fluids*, 10(4):224–229.

[Lesshafft et al.,] Lesshafft, L., Huerre, P., Sagaut, P., and Terracol, M. *Global Modes in Hot Jets, Absolute/Convective Instabilities and Acoustic Feedback*.

[Lin, 1946] Lin, C. C. (1946). On the stability of two-dimensional parallel flows: Part iii.—stability in a viscous fluid. *Quarterly of Applied Mathematics*, 3(4):277–301.

[Miksad, 1972] Miksad, R. W. (1972). Experiments on the nonlinear stages of free-shear-layer transition. *Journal of Fluid Mechanics*, 56(4):695–719.

[Monkewitz and Nguyen, 1987] Monkewitz, P. and Nguyen, L. (1987). Absolute instability in the near-wake of two-dimensional bluff bodies. *Journal of Fluids and Structures*, 1(2):165–184.

[Monkewitz et al., 1990] Monkewitz, P. A., Bechert, D. W., Barsikow, B., and Lehmann, B. (1990). Self-excited oscillations and mixing in a heated round jet. *Journal of Fluid Mechanics*, 213:611–639.

[Monkewitz and Sohn, 1988] Monkewitz, P. A. and Sohn, K. D. (1988). Absolute instability in hot jets. *AIAA Journal*, 26(8):911–916.

[Parekh et al., 1988] Parekh, D. E., Leonard, A., and Reynolds, W. C. (1988). Bifurcating jets at high Reynolds numbers. NASA STI/Recon Technical Report N.

[Provansal et al., 1987] Provansal, M., Mathis , C., and Boyer, L. (1987). Benard-vonkarman instability—transient and forced regimes. *Journal of Fluid Mechanics*, 182:1 – 22.

[Ranganathan and Govindarajan, 2001] Ranganathan, B. and Govindarajan, R. (2001). Stabilization and destabilization of channel flow by location of viscosity-stratified fluid layer. *Physics of Fluids - PHYS FLUIDS*, 13:1–3.

[Rayleigh, 1879] Rayleigh, L. (1879). On the stability, or instability, of certain fluid motions. *Proceedings of the London Mathematical Society*, s1-11(1):57–72.

[Raynal et al., 1996] Raynal, L., Harion, J., Favre-Marinet, M., and Binder, G. (1996). The oscillatory instability of plane variable-density jets. *Physics of Fluids*, 8(4):993–1006.

[Reynolds et al., 2003] Reynolds, W. C., Parekh, D. E., Juvet, P. J. D., and Lee, M. J. D. (2003). Bifurcating and blooming jets. *Annual Review of Fluid Mechanics*, 35(1):295–315.

[Sahu and Matar, 2010] Sahu, K. and Matar, O. (2010). Three-dimensional linear instability in pressure-driven two-layer channel flow of a newtonian and a herschel–bulkley fluid. *Physics of Fluids*, 22.

[Sahu and Matar, 2011] Sahu, K. and Matar, O. (2011). Three-dimensional convective and absolute instabilities in pressure-driven two-layer channel flow. *International Journal of Multiphase Flow - INT J MULTIPHASE FLOW*, 37:987–993.

[Sangalli et al., 1995] Sangalli, M., Gallagher, C. T., Leighton, D. T., Chang, H.-C., and McCready, M. J. (1995). Finite-amplitude waves at the interface between fluids with different viscosity: Theory and experiments. *Phys. Rev. Lett.*, 75:77–80.

[Schmid and Henningson, 2001] Schmid, P. J. and Henningson, D. S. (2001). *Stability and Transition in Shear Flows.*

[Schram and Hirschberg, 2003] Schram, C. and Hirschberg, A. (2003). Application of vortex sound theory to vortex-pairing noise: sensitivity to errors in flow data. *Journal of sound and vibration*, 266(5):1079–1–98.

[Selvam et al., 2007] Selvam, B., Merk, S., Govindrajan, R., and Meiburg, E. (2007). Stability of miscible core–annular flows with viscosity stratification. *Journal of Fluid Mechanics*, 592:23–49.

[Selvam et al., 2009] Selvam, B., TALON, L., Lesshafft, L., and MEIBURG, E. (2009). Convective/absolute instability in miscible core-annular flow. part 2. numerical simulations and nonlinear global modes. *Journal of Fluid Mechanics*, 618:323–348.

[Sreenivasan et al., 1989] Sreenivasan, K. R., Raghu, S., and Kyle, D. (1989). Absolute instability in variable density round jets. *Experiments in Fluids*, 7(5):309–317.

[Srinivasan et al., 2010] Srinivasan, V., Hallberg, M. P., and Strykowski, P. J. (2010). Viscous linear stability of axisymmetric low-density jets: Parameters influencing absolute instability. *Physics of Fluids*, 22(2):024103.

[Strykowski, 1986] Strykowski, P. J. (1986). *The control of absolutely and convectively unstable shear*. PhD thesis, Yale University.

[Strykowski and Niccum, 1991] Strykowski, P. J. and Niccum, D. L. (1991). The stability of countercurrent mixing layers in circular jets. *Journal of Fluid Mechanics*, 227:309–343.

[Strykowski and Niccum, 1992] Strykowski, P. J. and Niccum, D. L. (1992). The influence of velocity and density ratio on the dynamics of spatially developing mixing layers. *Physics of Fluids A: Fluid Dynamics*, 4(4):770–781.

[Strykowski and Sreenivasan, 1990] Strykowski, P. J. and Sreenivasan, K. R. (1990). On the formation and suppression of vortex 'shedding' at low reynolds numbers. *Journal of Fluid Mechanics*, 218:71–107.

[Taylor, 1923] Taylor, G. I. (1923). Viii. stability of a viscous liquid contained between two rotating cylinders. *Philosophical Transactions of the Royal Society of London. Series A, Containing Papers of a Mathematical or Physical Character*, 223(605-615):289–343.

[Todde et al., 2009] Todde, V., Spazzini, P. G., and Sandberg, M. (2009). Experimental analysis of low-reynolds number free jets. *Experiments in Fluids*, 47(2):279–294.

[Twiss, 1951] Twiss, R. Q. (1951). On oscillations in electron streams. *Proceedings of the Physical Society. Section B*, 64(8):654–665.

[Valluri et al., 2010] Valluri, P., NARAIGH, L. O., DING, H., and SPELT, P. D. M. (2010). Linear and nonlinear spatio-temporal instability in laminar two-layer flows. *Journal of Fluid Mechanics*, 656:458–480.

[Wille, 1963] Wille, R. (1963). Growth of velocity fluctuations leading to tur bulence in free shear flow,.

[Winant and Browand, 1974] Winant, C. D. and Browand, F. K. (1974). Vortex pairing : the mechanism of turbulent mixing-layer growth at moderate reynolds number. *Journal of Fluid Mechanics*, 63(2):237–255.

[Woods, 1969] Woods, J. D. (1969). On richardson's number as a criterion for laminar-turbulent-laminar transition in the ocean and atmosphere. *Radio Science*, 4(12):1289–1298.

[Wright, 2020] Wright, I. (2020).

[Yiantsios and Higgins, 1988] Yiantsios, S. G. and Higgins, B. G. (1988). Linear stability of plane poiseuille flow of two superposed fluids. *The Physics of Fluids*, 31(11):3225–3238.

[Yih, 1967] Yih, C.-S. (1967). Instability due to viscosity stratification. *Journal of Fluid Mechanics*, 27(2):337–352.

Appendix A

Calibration

A.1 Hotwire Anemometry

In order to establish a voltage-velocity relationship, the hotwire is calibrated against known velocities calculated from the rotameter readings and the corresponding voltage is measured from the hotwire. This produces a curve which shown in figure A.1.

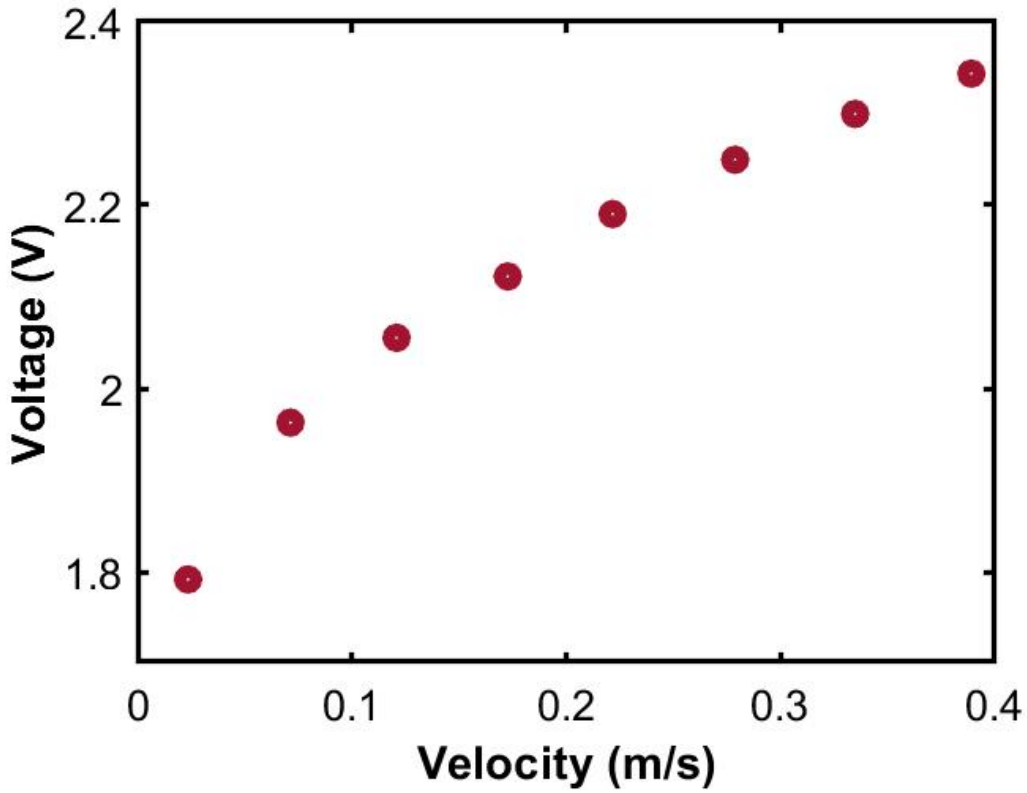

Figure A.1: Measured voltages corresponding to known velocities using the hotfilm probe

This curve is linearized using the generalized King's law and expressed as

$$E^2 = A + B * U^{1/n} \tag{A.1}$$

where E is the measured voltage, $A, B, \& n$ are constants found by curve fitting, and is shown in figure A.2.

U is the velocity of the jet found using

$$U = \frac{4Q}{\pi d^2} \tag{A.2}$$

where Q is the flowrate reading from the rotameter and d is the jet diameter. This assumes that the velocity profile is tophat in nature. In reality, the velocity profile deviates away from the ideal tophat profile due to the boundary layer thickness. Hence,

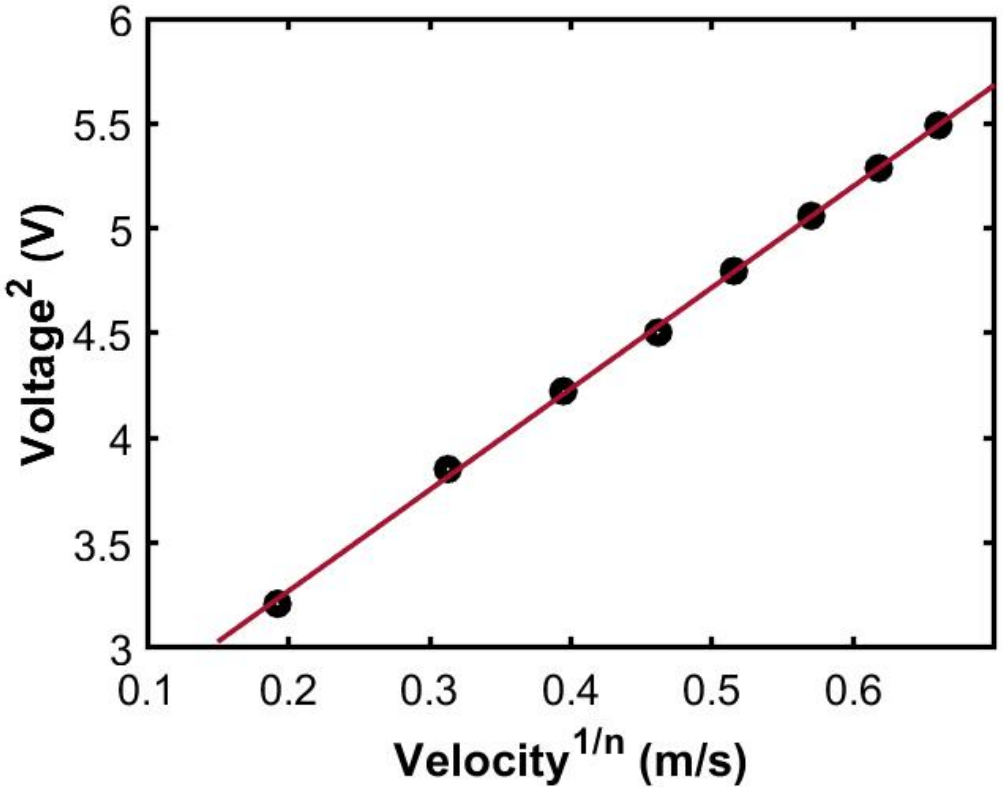

Figure A.2: Linearized velocity-voltage relationship

the centerline velocities are higher than what is calculated using equation A.2. To account for this correction, the volume issued by the actual measured velocity profile is compared to the volume of an ideal tophat profile. Note that in figure A.3 integrating the actual velocity profile in the θ direction from π to 2π gives the volume.

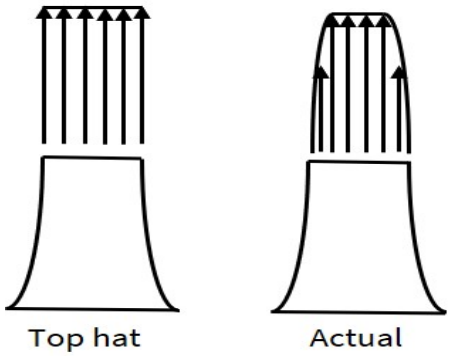

Figure A.3: Ideal tophat velocity profile (*left*) and real velocity profile (*right*)

A mismatch in volume is seen in figure A.4 and two correction factors, p_1 and p_2, are multiplied by A and B in equation A.1 such that the volumes are matched. The new calibration equation used for voltage-velocity conversions is expressed as

$$E^2 = p_1 A + p_2 B * U^{1/n} \tag{A.3}$$

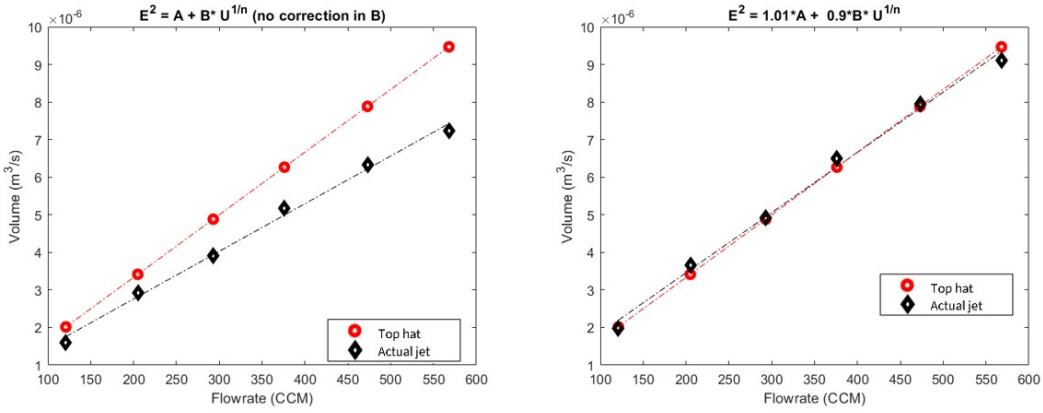

Figure A.4: Mismatch in volumes due to actual velocity profile (*left*) and corrected linear relationship (*right*)

This corrected equation is then used to convert all voltages into velocities.

A.2 Error Analysis

Errors in velocity measurements arise from errors in flowmeter readings, error in voltmeter readings, and the error associated with curve fittings and regressions. The flowmeter has a ±3% full scale accuracy, which corresponds to an uncertainty of ±0.023 m/s.

The uncertainty in the regression fit is calculated by:

$$\delta U = \frac{dU}{dE^2} = \frac{1}{n}\frac{E^2 - A^{\frac{1}{n}-1}}{B^2} \tag{A.4}$$

This corresponds to an uncertainty of 0.0011 m/s. The multimeter (Agilent 34411A) is the same as the one used in the previous study and has an uncertainty of 0.003% of reading and 0.005% of full scale. This corresponds to an uncertainty of ±0.000632 V for each reading.

The overall uncertainty in given by

$$\delta U = \sqrt{\delta U_{flowmeter}^2 + \delta U_{multimeter}^2 + \delta U_{regression}^2} \tag{A.5}$$

This results in an overall uncertainty of

$$\delta U = 0.026 m/s$$

in velocity measurements. Additionally, the frequency resolution is calculated to be 0.5 Hz for a sampling frequency of 2048 Hz over 2 seconds. Very close peaks ($f_1 - f_2 \approx 0.5$ Hz) are thus difficult to distinguish and are considered to be one. This however, does not affect the qualitative analysis of the flow.